Urban Climate 37 (2021) 100842

Contents lists available at ScienceDirect

Urban Climate

journal homepage: www.elsevier.com/locate/uclim

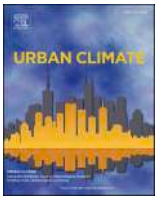

On the effect of sea breeze regime on aerosols and gases properties in the urban area of Rome, Italy

Annalisa Di Bernardino [a,*], Anna Maria Iannarelli [b], Stefano Casadio [b], Gabriele Mevi [b], Monica Campanelli [c], Giampietro Casasanta [c], Alexander Cede [d], Martin Tiefengraber [d,e], Anna Maria Siani [a], Elena Spinei [f], Marco Cacciani [a]

[a] Sapienza University of Rome, Department of Physics, Rome, Italy
[b] SERCO SpA, Frascati, Italy
[c] ISAC-CNR, Rome, Italy
[d] LuftBlick, Innsbruck, Austria
[e] University of Innsbruck, Department of Atmospheric and Cryospheric Sciences, Innsbruck, Austria
[f] Virginia Polytechnic Institute and State University, Department of Electrical and Computer Engineering, Blacksburg, VA, USA

ARTICLE INFO

Keywords:
Sea breeze
Urban aerosol
Air quality
Atmospheric boundary layer
Remote sensing

ABSTRACT

Several ground-based remote sensing and in-situ instruments were used to investigate the development of the sea-breeze front and its effect on both the optical and physical aerosol properties, the Particulate Matter (PM) content and the tropospheric and near-surface NO_2 concentrations. Most of the instruments belongs to the Boundary-layer Air Quality-analysis Using Network of Instruments (BAQUNIN) supersite, in the urban area of Rome (Italy). Two characteristic sea-breeze patterns were identified: the front days, in which the sea-breeze front develops in a few minutes, and the gentle breeze days, in which the onset of the front is gradual (more than 20 min). In the case of front days, Aerosol Optical Depth (AOD) increases during the onset of the breeze. The Ångström Exponent (AE), tropospheric and near surface NO_2 amounts are almost constant during the day, while the aerosols volume size distribution follows a trimodal distribution. $PM_{2.5}$ and PM_{10} concentrations decrease before the development of the sea-breeze front and then increase. Conversely, during gentle breeze days, AOD and AE do not change significantly. The tropospheric and near surface amount of NO_2, $PM_{2.5}$ and PM_{10} concentrations decrease, suggesting a significant dispersion of pollutants, while the aerosol size distribution shows a trimodal predominance.

1. Introduction

The Sea-Breeze (SB) regime is a well-known mesoscale circulation, primarily due to the horizontal pressure gradient between land and sea generated by the different heat capacities of water and dry land and by the different penetration depth of solar radiation in the subsurface medium (Simpson John, 1994). The SB starts to blow when the temperature difference between the sea and the nearby land is large enough to overcome any offshore synoptic wind. When cool, stable, marine air mass moves from the sea to the warmer inland, a quasi-steady state convective thermal internal boundary layer (TIBL) forms within the planetary boundary layer (PBL) and deepens

* Corresponding author.
E-mail address: annalisa.dibernardino@uniroma1.it (A. Di Bernardino).

https://doi.org/10.1016/j.uclim.2021.100842
Received 14 September 2020; Received in revised form 2 April 2021; Accepted 9 April 2021
2212-0955/© 2021 Published by Elsevier B.V.

with distance from the coastline. The horizontal boundary that marks the leading edge of cooler marine air is named SB front (Miller et al., 2003).

Since most of the large urban areas around the world arise in coastal areas and nearly half of the world's population resides within 150 km of the coastline (United Nations Atlas of the Oceans http://www.oceansatlas.org), it is essential to thoroughly investigate the development of the SB and its interaction with the urban environment. For example, it is crucial to plan the urban design of medium/large coastal cities, which are affected by both the Urban Heat Island (UHI) and the SB phenomena (Yoshikado, 1994; Yamamoto and Ishikawa, 2020), addressing the continuous urban development and foreseeing an eco-sustainable urban planning.

SB also affects the air quality of coastal regions (Simpson John, 1994). The upper limit of the breeze front, which coincides with the upper limit of the TIBL, acts as a lid severely limiting the vertical air mixing and the dispersion of pollutants, which remain confined within the shallow TIBL, resulting in an increase in their surface concentration. The amount of aerosol present in the atmosphere is directly related to the particle emission/production rates, to removal processes (such as sedimentation and precipitation scavenging), and to synoptic and local weather conditions. Information on aerosol characteristics is crucial from different perspectives, such as air chemistry (Meszaros, 1968), radiative effects (Charlson et al., 1967), and cloud microphysics (Ito, 1993). Several field campaigns have been carried out in order to evaluate the effect of SB on the urban environment (Cros et al., 2004; Melas et al., 1995) but the large diversity of pollutant sources, such as emissions from vehicular traffic, domestic combustion and industries, makes highly complex the analysis. The SB regime has been thoroughly studied in recent years by means of laboratory-scale experiments (Mitsumoto et al., 1983; Cenedese et al., 2000) and numerical simulations (Monti and Leuzzi, 2005; Ferdiansyah et al., 2020). Nevertheless, the effects on the optical and physical properties of the aerosol in the atmospheric boundary layer are still limited (Moorthy et al., 2003). Furthermore, the rapid variation of the most significant meteorological parameters and the time required for the establishment of SB must be taken into account for a detailed analysis in an urban context.

The ground-level emissions and the SB regime have a complex interaction in an urban environment, where also the spatial pattern of the urban canopy must be considered, and can profoundly modify the aerosol characteristics in terms of optical properties, size distribution, and composition. As found by Moorthy et al. (1993), the onset of the SB front has important effects on Aerosol Optical Depth (AOD) and columnar loading of aerosols on coastal locations. During SB events, the fine mode of the volume size distribution is more sensitive to continental air-mass types, while the coarse mode is more strictly governed by marine air masses. Boyouk et al. (2011) observed that in the coastal area of Dunkerque, France, $PM_{2.5}$ concentration increased with the SB onset because of the formation of the TIBL, with a maximum between 1 and 2 h after the front overpass. They found that the $PM_{2.5}$ amount was well correlated to the inverse of the mixing height, except during the passage of the SB front. Talbot et al. (2007), combining an experimental and a numerical approach, studied a sea-breeze system in a flat coastal area of the North Sea. They outlined that pollutants emitted outside the SB system were swept away and spread vertically by turbulent mixing during the passage of the SB front, with an increase in turbulence and maximal vertical ascents near the SB front. Thompson et al. (2007) used a numerical model to investigate the interaction between SB and complex coastal topography in New York City, US, characterizing the impact on near-surface contaminant concentrations. Their results show a change in plume direction and vertical re-distribution of pollutants: in particular, during the onset of the SB front, the upward motion depicts a decrease of the surface concentration while, after the passage of the front, surface concentrations quickly increase because pollutants are released within a shallow TIBL.

The timings of onset and end of the SB depend on both the local weather conditions and the background synoptic winds (Gahmberg et al., 2010). Moreover, large-scale meteorological conditions cannot be overlooked, as they dominate long-range aerosol transport. For example, Gkikas et al. (2012) investigated the synoptic conditions that favour the occurrence of aerosol episodes over the Mediterranean basin. They found frequent days with high aerosol concentrations during dry, warm periods, occurring when anticyclonic conditions prevailed over central Europe and the eastern Atlantic Ocean. In these cases, desert dust, anthropogenic pollution, and biomass-burning episodes are clearly identifiable and have significant effects on urban atmospheric conditions. In fact, as found by Meloni et al. (2007) and Senghor et al. (2020), the outbreaks of desert dust can attenuate UV and visible radiation, causing surface cooling (Di Sarra et al., 2002).

To the best of our knowledge, the effects of SB on aerosol and gases optical properties have been investigated only in industrial or coastal regions (Moorthy et al., 1993; Boyouk et al., 2011; Augustin et al., 2020). In this context, the primary objective of this work is the in-depth study of the meteorological variables that affect the SB front and its arrival in the urban area of Rome, with a focus on the different development SB patterns. Secondly, the impact of SB and synoptic circulation on columnar aerosol optical properties, aerosol vertical stratification, columnar NO_2 amount, particle size distribution, and ground level PM concentrations are also analysed. Particularly, NO_2 is primarily emitted by burning fuel at high temperature and exhaust of motor vehicle and has a relatively short photochemical life, assuming minima values during summer days (2–6 h, Beirle et al., 2011) and maximum in winter (12–24 h, Beirle et al., 2003). According to the report of Air Quality Europe 2019 (https://www.eea.europa.eu/publications/air-quality-in-europe-2019), the NO_2 concentration is closely related to local traffic sources even if its seasonal cycle depends also on the meteorological conditions and the solar zenith angle. This allows the tropospheric columnar content to be considered as a proxy of the content within the PBL.

The paper is structured in five Sections. In Section 2, the location and the ground-based remote sensing instruments are described. In Section 3, the criteria used for detection and classification of the SB days are given, providing the description of the typical weather conditions of a day in which the SB does not reach the urban area and focusing on two distinct SB patterns. A summary of the results and the main conclusions are presented in Sections 4 and 5, respectively.

Fig. 1. Geographical map of the area of interest (left), BAQUNIN supersite urban location (right) and BAQUNIN supersite panoramic view (bottom). Red line and yellow stars identify the urban boundaries of Rome and BAQUNIN site, respectively. (For interpretation of the references to colour in this figure legend, the reader is referred to the web version of this article.)

2. Location and instrumentation

The city of Rome is located about 27 km inland from the Tyrrhenian coast. The proximity of the urban area to the sea makes local circulation complicated, due to the presence of complex orography surrounding the city, the SB circulation and its interaction with UHI (Colacino, 1982; Ferretti et al., 2003; Pelliccioni et al., 2015). As shown in previous studies, the city is subject to sea-breeze circulation throughout the entire year (Petenko et al., 2011), but more frequently during summer, when the high temperatures and the anticyclonic conditions, typical of the Mediterranean region, increase the difference in temperature between the sea surface and the land, favouring the triggering of the SB.

Along the Tyrrhenian coast of the central region of Italy, during nighttime the wind is mostly northerly because of the drainage effect from the bottom of the Tiber valley in conjunction with large-scale circulation. Differently, during daytime when the SB occurs, the wind blows from South-West and remains constant in direction for several hours. Petenko et al. (2011) demonstrated that the aforementioned wind diurnal cycles are well detectable in the rural surroundings of the Rome area: during nighttime, wind blows from the sector from North to East-North-East or from East and Southeast. The large-scale flow at higher altitudes above the orography governs the occurrence of one or the other pattern in the daily evolution of the near-surface wind. Colacino (1982) found that the SB could penetrate inland up to 50 km from the coastline, reaching a vertical development of about 1000 m. Typically, the SB front reaches the urban area between 11:00 and 13:00 UTC.

In this work, ground-based observations are mostly carried out at the BAQUNIN (Boundary-layer Air Quality-analysis Using Network of Instruments, 41.902 N, 12.516 E, https://www.baqunin.eu/, Iannarelli et al., 2021) supersite urban location (with the exception of the atmospheric pressure and PM concentrations, as explained in the following). The site is hosted by the Physics Department of Sapienza University of Rome and is located in the Rome city centre, in a densely built-up area, which can be considered representative for the study of urban micro-meteorological and pollution conditions (Pichelli et al., 2014; Pelliccioni et al., 2020). All instruments are located on the rooftop of the building, to have negligible local effects related to the urban arrangement. A map of the area, including the location and a panoramic view of the measurements site, is given in Fig. 1.

In what follows, a brief description of the instruments and quantities used in this study is provided.

A three-axial, monostatic Doppler SODAR with a pulse repetition rate of 1 s operates continuously providing information about the atmospheric thermal turbulence (i.e. the turbulence caused by solar heating of the surface, which in turn heats the lower atmosphere resulting in uneven convective currents), as well as the horizontal wind speed and direction with a maximum probing range of 230 m a.s.l.. Two of the three antennas are tilted 20° from the zenith, pointing North and East, while the third points vertically. The acoustic bursts (centred on 4450.75, 4650.75 and 4840.75 Hz, 0.1 s long) permit the retrieval of the atmospheric thermal turbulence and the horizontal wind profiles with a vertical resolution of about 1.4 m and 5.7 m, respectively. Details on the retrieval procedure can be found in Mastrantonio and Fiocco (1982) and Mastrantonio et al. (1994). Horizontal wind speed (U) and direction (θ) temporal trend have been computed considering all the valid wind data measured at the first valid range gate (about 84 m.a.s.l), discarding the closest to the rooftop, which is often affected by electro-acoustic transducer membrane ringing.

A ground-based meteorological station (Vaisala Weather Transmitter WXT520), belonging to the national private network of certified quality urban weather stations “Climate Network” and managed by the OMD Foundation (Fondazione Osservatorio Milano Duomo, https://www.fondazioneomd.it/), provides air temperature (T) and relative humidity (RH) with a temporal resolution of 10 min.

The atmospheric pressure has been measured by a Davis Vantage Pro 2 weather station, belonging to the meteorological regional network “Meteo Lazio” (https://www.meteoregionelazio.it/) and located about four kilometres away from the BAQUNIN supersite (41.890 N, 12.560 E). It has been used, together with T and RH values - measured by the aforementioned ground-based meteorological station - for the evaluation of the specific humidity (q) (Wallace and Hobbs, 2006) profiles with 10-min resolution.

The SR11 pyranometer (Azouzoute et al., 2019) collects the solar radiation in the 285–3000 nm spectral range received by a plane surface from a 180° field of view angle every 10 s. The comparison between the solar radiation provided by the pyranometer and the weather parameters provided by the meteorological station allowed the identification of clear-sky days.

The Cimel CE318-T radiometer, belonging to the AERONET-EUROPE network (https://aeronet.gsfc.nasa.gov/, Giles et al., 2019), and the Prede–POM sky radiometer, belonging to SKYNET/ESR network (http://www.euroskyrad.net/, Campanelli et al., 2012) perform measurements of direct and diffuse solar radiation at different wavelengths (340, 380, 440, 500, 675, 870, 940, 1020 and 1640 nm for Cimel CE318-T, and 340, 400, 500, 675, 870, 940 and 1020 nm for Prede-POM). All the wavelengths (except 940 nm) are used to estimate columnar aerosol optical properties as AOD, Ångström wavelength exponent (AE) and volume size distributions. AOD and AE time resolution is about 10 min for Cimel CE318-T, and 1 min for Prede–POM; volume size distributions are obtained by inversion of the diffuse solar radiation measurements. Their time resolution depends on both the time interval of measurements (20 min for Cimel CE318-T and 10 min for Prede–POM) and the quality check performed on the products of the inversion, which in some cases strongly reduces the number of available distributions. The Cimel CE318-T 940 nm wavelength is also used to estimate the total column water vapour (TCWV). AERONET products are obtained from Version 3.0, Level 1.5 analysis (Giles et al., 2019), whereas ESR/SKYNET products are from SUNRAD, Level 1.0 (Estellés et al., 2012) and Skyrad pack version 4.2, Level 1.0 analysis (Nakajima et al., 2020).

The Pandora 2S spectrometer, belonging to the Pandonia Global Network (PGN, https://www.pandonia-global-network.org/, Cede, 2019; Cede et al., 2019), performs measurements of direct and diffuse solar radiation in the spectral range 290–900 nm using two spectrometers. This instrument is used to estimate total column, tropospheric column and near surface concentration of several gases. In the present work, tropospheric columns and near surface concentration of nitrogen dioxide (NO_2) with assured instrumental high quality are used. Data, with a temporal resolution of about 8 min, were analysed using PNG standard retrieval code, applying a fitting

Table 1
Errors are the sum of systematic and statistical uncertainties. Errors for U, θ, tropospheric and surface NO_2 are determined as one standard deviation uncertainties.

Parameter	Units	Uncertainty	Reference
Wind velocity (U)	m/s	0.26	Casasanta et al., 2021
Wind direction (θ)	°	12.1	Casasanta et al., 2021
Air temperature (T)	°C	0.30	Vaisala data sheet
Total column water vapour (TCWV)	%	7.5	Pérez-Ramírez et al., 2014
Specific humidity (q)	%	3.0	Vaisala data sheet
Aerosol optical depth (AOD)	%	2.0	Campanelli et al., 2007
Tropospheric and near surface NO_2	%	5–30	Cede, 2019; Spinei et al., 2021
PM_{10} and $PM_{2.5}$	$\mu g/m^3$	0.30	FAI Instruments data sheet

window from 435 to 490 nm (Spinei et al., 2021).

Finally, the Regional Environmental Protection Agency (ARPA) of Lazio region provided the hourly PM_{10} and $PM_{2.5}$ (corresponding to the mass concentration of particulate matter with an aerodynamic diameter less than 10 μm and 2.5 μm, respectively) concentrations measured in the urban air quality station located in Rome city centre (41.910 N, 12.496 E). PM_{10} and $PM_{2.5}$ levels were automatically collected using a SWAM 5a Dual Channel Monitor (FAI Instruments, Fonte Nuova, Rome, Italy). The PM mass concentration is determined by the beta attenuation technique (Macias and Husar, 1976).

In order to investigate the impact of meteorological measurements on aerosol optical characteristics, weather data with high frequency were homogenized in terms of temporal resolution by averaging all parameters over intervals of 10 min. In this way, the development and evolution of the sea breeze front can be correctly captured, also analysing gradients and maintaining low computational costs. Otherwise, the investigation of aerosols and gases characteristics have been carried out maintaining the original temporal data resolution. For this reason, in the case of low frequency measurements, such as those derived from ARPA station, results regarding these data should be taken with a degree of caution. In Table 1, the available uncertainties on the variables are summarized. In the analysis of the results, uncertainties are also depicted by means of graphical error bars.

3. Detection of sea breeze events

As explained in the previous Section, the Rome area is often subject to the inland penetration of the SB regime, especially during summer. The following subsections discuss in detail what happens when the SB front reaches the city centre. Anyway, first, it is interesting to discuss a day in which the SB front fails to develop up to the urban area. This condition occurs more frequently in the winter season.

For this reason, Fig. 2 shows the reference meteorological quantities relating to 24 November 2019, chosen as an example day. Fig. 2a shows the vertical wind profile measured by the SODAR, while in Fig. 2b the temporal evolution of wind speed and direction measured by the SODAR at its first useful range gate (i.e. 84 m.a.s.l.) is depicted. Throughout the day, the wind speed is below 4 m/s (maximum between 00:00 UTC and 02:00 UTC and between 08:00 UTC and 10:00 UTC), with a daily average velocity of approximatively 1.5 m/s. The prevailing daily wind direction is North-North-East. Only between 14:00 UTC and 16:00 UTC the wind direction changes and the wind blows from South and West. In the late afternoon, wind blows again from North. The hemispherical solar radiation measured by the pyranometer (Fig. 2c) shows a maximum of about 400 W/m^2, ensuring the absence of clouds and rain during the day. The ground temperature, illustrated in Fig. 2d, increases up to about 11:30 UTC, i.e. in correspondence of the maximum solar radiation and oscillates around the maximum value (19 °C) up to 14:00 UTC. In the afternoon, T decreases down to about 12 °C during the following night. The oscillatory trend of the temperature in the central hours of the day (11:00–14:00 UTC) is also confirmed by the derivative of the temperature, shown in the same figure. Unfortunately, only a few measurements of total column water vapour are present all over the day. The available data have an almost constant value (between 1.6 and 1.9 cm) up to about 12:30 UTC. Nonetheless, due to the lack of data, no conclusions can be drawn on the daily trend. Fig. 2e presents the evolution of specific humidity, q. It decreases during the night and the morning hours, passing from about 4.7 cm at approximatively 01:00 UTC down to 3.5 cm at about 12:50 UTC. Then, q oscillates around 3.6 cm and, starting from 15:00 UTC, it increases again reaching the night values at 19:00 UTC.

The identification of SB events can be carried out using different manual or objective methods (Azorin-Molina et al., 2011; Cafaro et al., 2019) taking into account several meteorological variables. Some of these are connected to the passage of SB (such as wind speed and direction, specific humidity, total column water vapour and air temperature), others are linked to the structure and the development of the SB front itself (e.g. cloudiness and precipitations). However, these methods are strictly related to the nature and morphology of the region under investigation.

In this study, the following criteria, based on local and synoptic weather conditions as suggested in Azorin-Molina et al. (2011), were adopted for the detection and classification of the SB days: (i) clear days with high-pressure systems, with no rainfall recorded in the time window relevant to the sea-breeze passage; (ii) change in surface wind direction and wind intensity some hours after sunrise, with the wind blowing from the sea to the land, perpendicularly to the coastline; (iii) increase in specific humidity and content of total column water vapour, associated with a simultaneous decrease in the atmospheric temperature because of cooler, moister air coming from the sea.

Although the breeze regime has been observed in the Rome area in all seasons, this study focuses on summer observations, in order to capture more intense and significant events. In particular, June, July and August 2018 and 2019 have been selected to have a

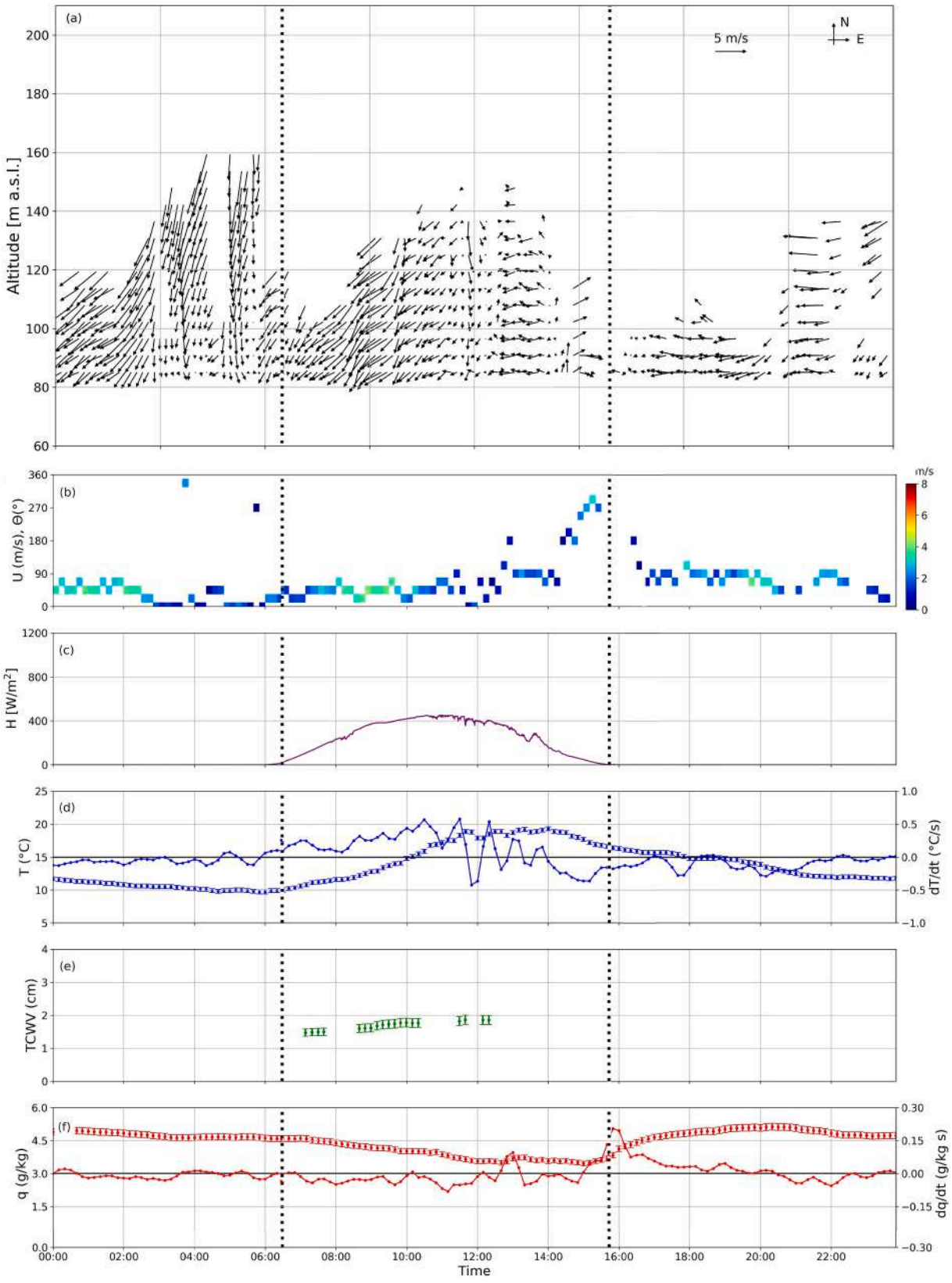

(caption on next page)

Fig. 2. Temporal variation of meteorological parameters for 24 November 2019. (a) 10-min averaged vertical profiles of horizontal wind velocity, (b) wind velocity U (colours) and direction θ as measured by SODAR at 84 m.a.s.l, (c) hemispherical solar radiation, (d) ground air temperature T, (e) total column water vapour TCWV, (f) specific humidity q. Continuous lines in panels (d) and (f) refer to the gradient of T and q, respectively. The black dotted lines show the sunrise and the sunset.

statistically significant number of events under examination and to evaluate the peculiar characteristics of the phenomenon based on the synoptic weather conditions.

During the observation period (June, July and August of 2018 and 2019), 48 days of SB that meet the criteria listed above were identified. Two characteristic patterns were observed, closely related to the development of the SB front and its impact on the urban centre. In both cases, in the urban station, wind blows from South-West and the surface wind speed exceeds 5 m/s, but the variation of ground air temperature, total column water vapour and specific humidity in correspondence of the onset of the SB show different behaviours.

The first pattern, hereinafter named “front days”, is the case in which the SB front is well detectable, thanks to the sharp change of surface meteorological quantities (such as wind intensity and direction, air temperature, total column water vapour and specific humidity) typically occurring in less than 20 min. This case includes days in which the variation of total column water vapour and specific humidity is greater than 10%, and that of air temperature is greater than 5%, with respect to the pre-front values.

The second configuration, hereinafter defined as “gentle breeze days”, is characterized by a slow and gradual onset of the SB, without a net increase in atmospheric total column water vapour and specific humidity and decrease of surface air temperature. Typically, this change occurs in at least 20 min. Since in this case the variations of T and q are not particularly marked, in the following graphs the temporal derivatives of these variables (expressed in °C /s and g/Kg s, respectively) are used to better highlight their increase/decrease.

The development of the sharp SB front is typically related to synoptic weather conditions and coastline orientation. As argued by Hunt and Simpson (1982), when the prevailing winds are offshore, there is a clear formation of the SB convergence area due to the reversal of wind direction from offshore to onshore. Simpson John (1994) concluded that, given an adequate gradient of temperature between sea and land, the development of the SB front depends on the balance between converging winds, acting to form the front, and the vertical mixing over the land, acting to block its formation. In addition, numerical simulations (Srinivas et al., 2006) and in-situ observations (Atkins et al., 1995) confirmed that the SB front is stronger in the case of seaward wind direction, with higher gradients of air temperature and moisture and faster inland propagation than the onshore events.

In Figs. 3 and 4, the daily variations of the atmospheric quantities typically involved in the development of the SB are shown. According to our SB front definition, the orange dashed vertical line represents the arrival of the SB front at the BAQUNIN site, while the orange-filled area depicts the time interval required for the passage of the front and the steady establishment of the SB (Simpson John, 1994). Black, dotted lines depict the sunrise and sunset times of the days examined.

Fig. 3 refers to 1 August 2019, belonging to the SB “front days” category. The SB front onsets at 12:00 UTC and fully develops in about 20 min. Fig. 3a shows the 10-min averaged vertical profiles of SODAR wind speed (U) and wind direction (θ). The change in wind direction and intensity is clearly detectable. In fact, during nighttime, the wind blows predominantly from Northeast (i.e. from inland, as expected in the case of land breeze regime); wind direction changes about 20 min after the sunrise and, for the whole duration of the SB event (i.e. from 12:00 UTC up to 16:30 UTC), remains almost constant. Because the coastline in the central region of Italy is Northwest-Southeast oriented, during SB events wind blows from the South-West quadrant, i.e. with a direction between 180° and 270° (clockwise) with respect to the North. The vertical wind speed profiles show that, at 12:00 UTC, the wind direction is not homogeneous along the vertical, due to the passage of the SB front. In fact, a direction of 200° up to about 130 m.a.s.l., and about 215° above this altitude is distinguished. This quote can be approximatively considered as the top of the TIBL. At 12:20 UTC, i.e. when the front is fully developed, the wind direction is constant along the vertical and equal to about 200°. As demonstrated by Colacino (1982), the breeze front on Rome can reach an altitude of about 1000 m.a.s.l. and therefore only a first qualitative analysis on the development of the TIBL can be carried out using SODAR data.

As shown in Fig. 3a and b, as soon as the SB front develops, the wind velocity significantly increases, passing from 2 m/s up to 8 m/s. In Fig. 3c, d, e and f the temporal evolution hemispherical solar irradiance (H), surface temperature (T), total column water vapour (TCWV), and surface specific humidity (q) are shown. The continuous lines in Fig. 3d and f represent the T and q gradients. The hemispherical radiation diurnal trend, provided by the pyranometer, ensures that the sky is clear and that, hence, the variation of the other meteorological quantities is associated to the arrival of the breeze and not to changes in other meteorological conditions such as, e.g., cloud formation or precipitation. As highlighted by the orange-filled region, a decrease in ground air temperature of about 1 °C occurs. The TCWV assumes almost constant values (about 1.97 cm) before the establishment of the SB (up to 12:00 UTC) and shows a marked increase when the front onsets, reaching 3.08 cm (at 12:20 UTC). After the complete development of the SB, TCWV remains quite constant, with a decrease from 16:10 UTC, i.e. when also the wind intensity decreases. The ground specific humidity, as expected on a warm, high-pressure day, is quite constant during nighttime (about 6.5 g/kg) and decreases at sunrise, reaching minima values in correspondence of the maximum of solar irradiance. After sunrise and before the onset of the front, q reduces, passing from 6 g/kg at 5:00 UTC up to 3.1 g/kg at 12:00 UTC as convection entrains drier air from above the atmospheric boundary layer. When the SB front develops, q has a noticeable increase because of the advection of moister air from the sea, going from 3.1 g/kg up to 4.6 g/kg in 20 min. When the SB circulation is established, the q value fluctuates around approximately 4 g/kg, while, when the SB vanishes (i.e., at about 16:30 UTC), q increases again until the typical nighttime value. In agreement with evidence by Ahrens (2012) and Moorthy et al. (1993), unlike what happens for q and TCWV, the decrease in temperature is observed just after the complete development of the SB

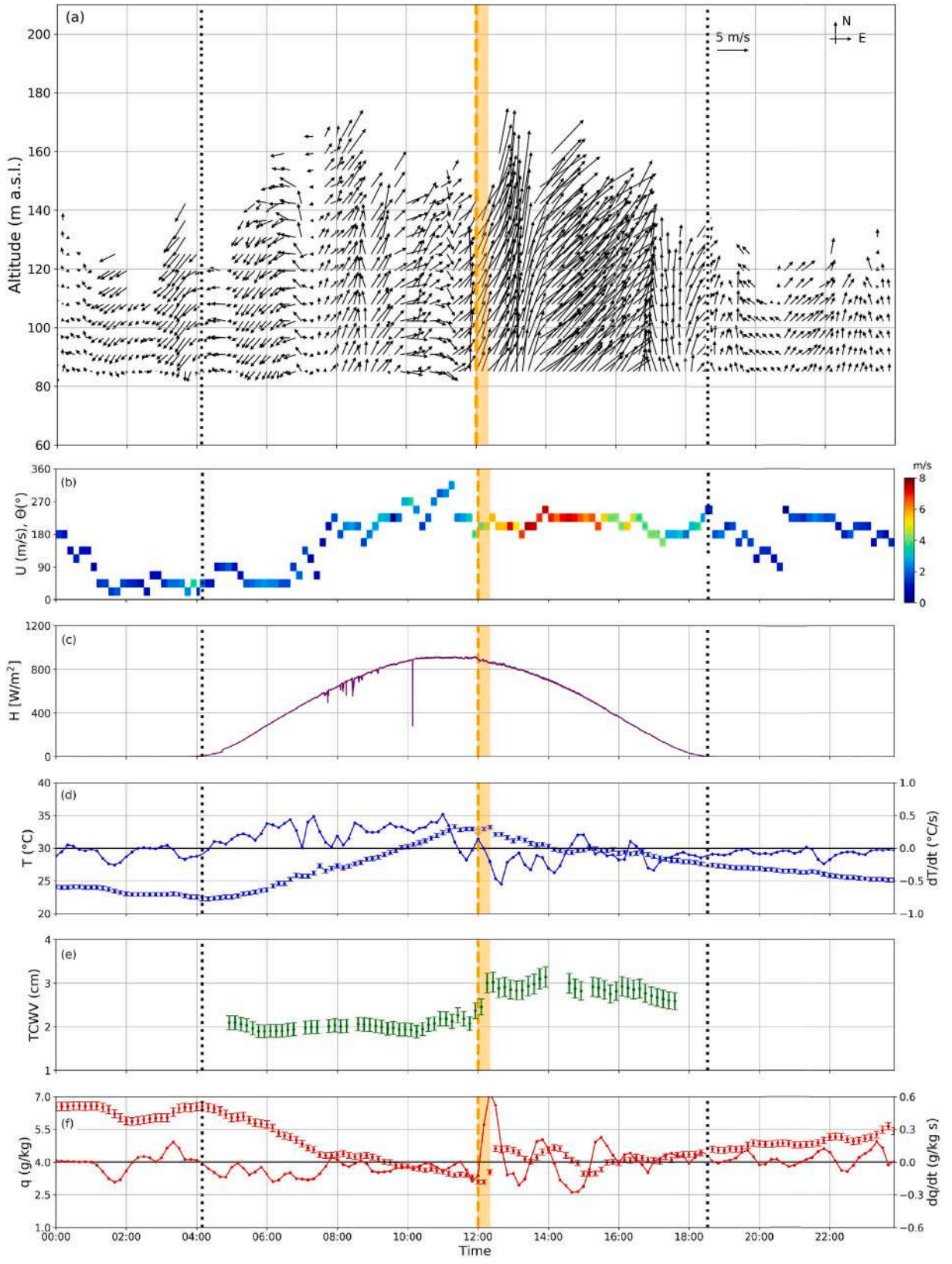

(caption on next page)

Fig. 3. Temporal variation of meteorological parameters for 1 August 2019. (a) 10-min averaged vertical profiles of horizontal wind velocity, (b) wind velocity U (colours) and direction θ as measured by SODAR at 84 m.a.s.l, (c) hemispherical solar radiation, (d) ground air temperature T, (e) total column water vapour TCWV, (f) specific humidity q. Continuous lines in panels (d) and (f) refer to the gradient of T and q, respectively. The orange dashed line represents the arrival of the SB front. The orange-filled area depicts the time interval required for the complete development of the SB. The black dotted lines show the sunrise and the sunset.

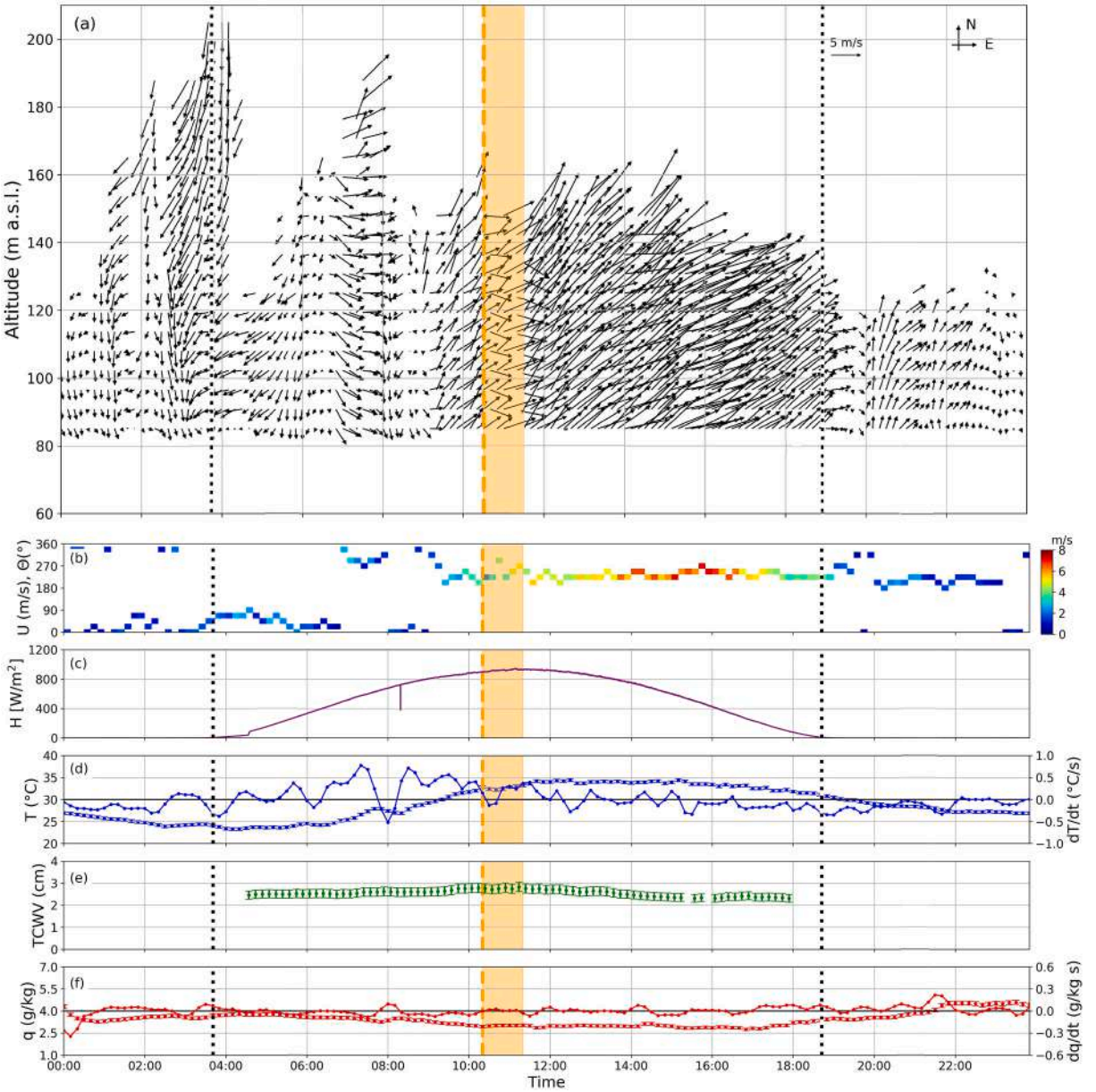

Fig. 4. Temporal variation of meteorological parameters for 2 July 2019. (a) 10-min averaged vertical profiles of horizontal wind velocity, (b) wind velocity U (colours) and direction θ as measured by SODAR at 84 m.a.s.l, (c) hemispherical solar radiation, (d) ground air temperature T, (e) total column water vapour TCWV, (f) specific humidity q. Continuous lines in panels (d) and (f) refer to the gradient of T and q, respectively. The orange dashed line represents the arrival of the SB front. The orange-filled area depicts the time interval required for the complete development of the SB. The black dotted lines show the sunrise and the sunset.

and not in conjunction with its onset.

Fig. 4 refers to 2 July 2019, a typical "gentle breeze" day. Like the case of SB front days, before the SB onset the wind blows from the Northeast quadrant (land breeze), with typical intensity near the ground lower than 2.5 m/s. The SB develops at 10:30 UTC, when the

Table 2
List of SB patterns and their occurrence.

SB pattern	Occurrence
Front days	19
Gentle breeze days	17
Gentle breeze days after at least 48 h of prevailing synoptic weather conditions	12

change of wind direction and the increase in wind velocity are clearly visible (Fig. 4a) but the variations are slower and take about one hour. When the arrival of the SB front is not well discernible, the change in wind direction (Fig. 3b) can also take place about one hour before the onset of the SB. In this period, however, the wind speed remains rather low ($U < 3$ m/s). However, in this case, the SB circulation can be considered as fully established when a clear increase in U (>5 m/s) occurs not only near the ground but also over the entire wind vertical profile. Gentle breeze days are characterized by very small gradients in temperature, TCWV, and specific humidity. This trend is clearly visible in Fig. 4d, e, and f: all meteorological quantities follow the behaviour they should have with the arrival of the breeze, but gradients are very low. Again, the hemispheric solar radiation trend, collected by the pyranometer (Fig. 4b), ensures that there are no clouds and precipitation.

The diurnal trends of meteorological quantities are in accordance with the SODAR measurements used by Mastrantonio et al. (1994) in the study on the urban area of Rome. Moreover, meteorological quantities agree with the results by Moorthy et al. (1993) and Boyouk et al. (2011), despite their locations being coastal, without significant obstacles near the measurement site. Moorthy et al. (1993) found a double behaviour of the breeze, confirming that the classification in front and gentle breeze days does not depend on the orography of the region or on the local circulation. As suggested by Hunt and Simpson (1982), the differences in the development of the SB front are essentially related to the direction and intensity of the synoptic wind. When the prevailing winds are offshore (e.g from the land), as for 1 August 2019, the reversal of winds from offshore to onshore is associated with the formation of a convergence zone that can give rise to a sharp boundary SB front. Otherwise, when the wind direction changes before the onset of the breeze (as for 2 July 2019), the convergence zone does not develop sufficiently and, consequently, the front is not particularly intense and recognizable. Unfortunately, no PBL height measurements are available at BAQUNIN on the analysed days, so the development of the TIBL can only be detected qualitatively when the onset of the SB is sharp. It would be very interesting to deepen the topic using data from LIDAR and ceilometer, which can provide detailed information on the development of the PBL height and, consequently, of the TIBL.

In the central region of Italy, both SB front patterns are important. In fact, the occurrence of the front days is comparable with the gentle breeze days: in the dataset used in this study, 60% of cases are characterized by the gradual onset of the breeze, while the remaining 40% belongs to “front days” (Table 2).

4. Effects on urban aerosols

4.1. Front days

The temporal variation of the AOD measured by Prede–POM at the representative wavelength of 500 nm for a typical SB front day is shown in Fig. 5a. Except for minor fluctuations, the AOD shows constant values (about 0.1) after sunrise and in the early morning of 1 August 2019. In agreement with results by Moorthy et al. (1993), during the development of the SB front, a net increase in AOD is detectable (about 30–35% in this study between 11:50 UTC and 12:20 UTC). A first appreciable increase is present at 10:30 UTC while, a few minutes before the arrival of the front, the AOD decreases slightly. Moorthy et al. (1993) found a sharp increase in AOD about 12 min after the onset of the front while, in the present study, the AOD starts to increase about 10 min preceding the onset of the breeze (11:50–12:00 UTC), i.e. immediately before the development of the front. This dissimilarity can be attributed to the different conformation of the investigated regions: Moorthy et al. (1993), in fact, conducted their study on a coastal, flat area while, in the present case, the effects of the urban canopy and anthropogenic sources are substantial. When the SB is fully developed, i.e. about 20 min after the onset of the front, the AOD reaches about twice the pre-front values and appears steadier. It remains almost constant until the SB ends and increases again in the late afternoon (reaching values of about 0.24 at 16:30 UTC). Furthermore, the lack of AOD data during the development of the SB front indicates that the SUNRAD inversion algorithm discarded the measurements. In agreement with the slight decrease in H (Fig. 3b) and with the increase in q shown in Fig. 3f, this is attributable to the appearance of a light layer of clouds that often accompanies the arrival of the breeze front.

During the front days, the AE is not affected by the arrival of the SB front. In fact, although its trend throughout the day is decreasing, during the onset of the breeze no significant changes can be appreciated. Also in this case, the absence of data in the interval 12:00–12:20 UTC does not allow to draw conclusions on what happens during the development of the front. The AE remains almost constant when the breeze is steady, with a decrease of about 10%, while it decreases considerably when the breeze fades out.

Fig. 5b and c show the temporal variation of Pandora-2S tropospheric column and near-surface NO_2 amount, respectively. These quantities are estimated from multi-axis sky measurements at six different azimuth angles. The observed small cyclic variations in concentrations are mainly due to inhomogeneity of the NO_2 field for different viewing angles. Despite this, in this work, all data have been considered as representative of the investigated site. In the urban environment, tropospheric and surface NO_2 amounts are mainly related to vehicular emission and anthropogenic activities (see, e.g., Schreier et al., 2020; Mavroidis and Chaloulakou, 2011). The impact of the SB on NO_2 near surface and columnar loads appears to be not easily detectable. In fact, while NO_2 concentrations retrieved at different azimuth angles decrease in correspondence of the SB onset, the quantification of the SB effects requires a rigorous

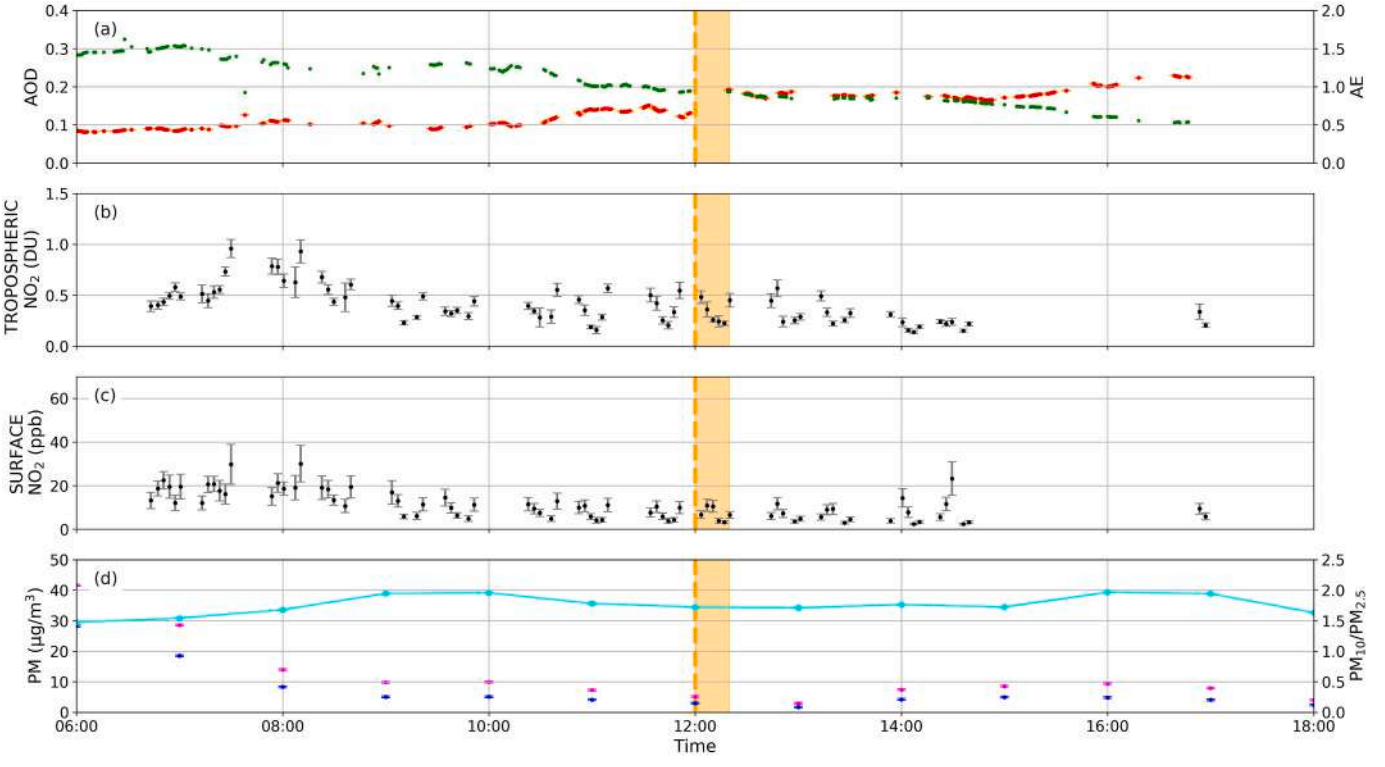

Fig. 5. Daily variation of (a) AOD (red dots) and AE (green dots), (b) tropospheric and (c) surface NO_2 amount, (d) PM_{10} (purple dots) and $PM_{2.5}$ (blue dots) concentration and $PM_{10}/PM_{2.5}$ ratio (cyan line) on 1 August 2019. Vertical bars depict measurement errors. The orange dashed line represents the arrival of the SB front. The orange-filled area depicts the time interval required for the complete development of the SB. (For interpretation of the references to colour in this figure legend, the reader is referred to the web version of this article.)

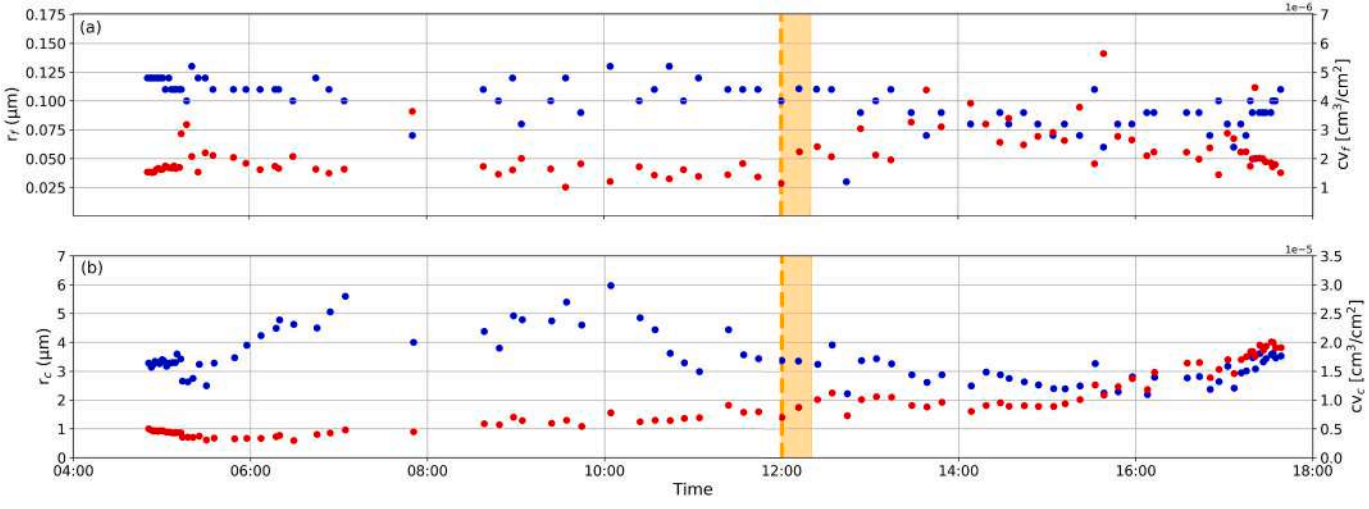

Fig. 6. Daily variation of modal radius (blue) and concentration values (red) for (a) fine and (b) coarse aerosols on 1 August 2019. The orange dashed line represents the arrival of the SB front. The orange-filled area depicts the time interval required for the complete development of the SB. (For interpretation of the references to colour in this figure legend, the reader is referred to the web version of this article.)

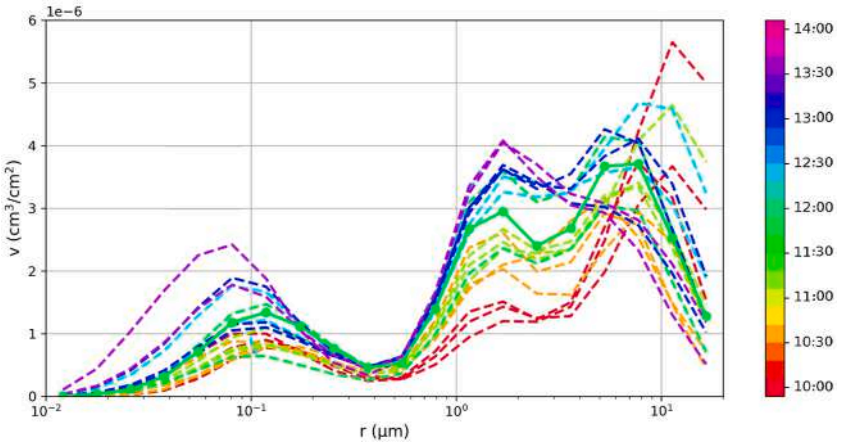

Fig. 7. Daily variation of volume size distribution on 1 August 2019 (from 10:00 up to 14:00 UTC). Marked line refers to the first series after the SB onset.

analysis of horizontal inhomogeneity and photochemistry. This topic is currently being investigated by the scientific community (Drosoglou et al., 2017; Drosoglou et al., 2018) and, given the peculiarities and geographical position of the city of Rome, it will be the subject of future studies. Tropospheric NO_2 assumes values between 0.2 and 0.6 DU, while near-surface NO_2 concentration ranges from 4 and 11 ppb.

The daily variation of PM_{10} and $PM_{2.5}$ is shown in Fig. 5d. A decrease in PM_{10} and $PM_{2.5}$ is simultaneously observed before the SB onset while, from 13:00 UTC, both components show a net increase (from 2 to 4 $\mu g/m^3$ and from 3 to 8 $\mu g/m^3$ for PM_{10} and $PM_{2.5}$, respectively). As found by Rimetz-Planchon et al. (2008), the increase in PM concentration after the establishment of SB is related to different factors. First, the TIBL lowers the height of the atmospheric boundary layer and, consequently, reduces the volume of air available for aerosols mixing. Moreover, the advection of cooler, humid marine air modifies the gas-particle conversion rate, because of the effect of turbulence mixing across temperature and humidity gradient between sea and land (Easter and Peters, 1994; Crumeyrolle et al., 2010) and brings sea-salt over the urban region.

The PM ratio trend differs from the results by Boyouk et al. (2011), who found that, during the SB front development, a simultaneous increase in PM_{10} and $PM_{2.5}$ occurs and the change in PM ratio indicates the advection of large particles. In our case, as shown in Fig. 5d, the $PM_{10}/PM_{2.5}$ ratio is not affected by the passage of the front. Such a different behaviour can be related to the peculiarities of the geographic areas considered in the studies: in fact, Boyouk et al. (2011) focused on a coastal, industrial area where the continuous production of PM due to vehicular traffic and anthropic activities was limited. Moreover, in the present study particulate matter results must be considered with a certain degree of caution. In fact, these data have an hourly temporal resolution, i.e. lower than the other quantities considered, thus not allowing for a detailed characterization of the effects of the SB front on ground PM concentration.

Related to the same day, Fig. 6a shows the temporal variation of the modal radius (r_f) and concentration values ($c_{v,f}$) of fine aerosol component, computed considering particles greater than 0.5 μm as a unique coarse mode. r_f remains almost constant (about 0.11 μm) until 7:00 UTC and oscillates between 0.08 μm and 0.12 μm from 9:00 UTC to 11:00 UTC. At the turn of the onset of SB front (11:20 UTC - 12:40 UTC), r_f assumes an almost constant value (about 0.11 μm) but $c_{v,f}$ increases from a value of about 1×10^{-6} cm^3/cm^2 just before the onset of SB, up to 2.5×10^{-6} cm^3/cm^2 when the SB is established. The increase of volume concentrations of fine particles and their stable radius shows the greater number of fine particles in the atmosphere, transported by the SB.

The temporal variation of the aerosol coarse mode in Fig. 6b shows that the coarse modal radius (r_c) increases during the early morning (up to 07:00 UTC) passing from 3 μm up to 5 μm, remains almost constant (about 5 μm) from 07:00 UTC up to 10:00 UTC and decreases in the time range 10:00 UTC – 11:10 UTC, passing from 6 μm up to 3 μm. Then, it assumes almost constant values from about one hour before the arrival of the SB front (about 3.5 μm) until about 13:30 UTC. The corresponding coarse mode width (not shown in the graphs) increases significantly at about 08:00 UTC (with values between 0.9 and 1.05), confirming that the coarse mode assumes a bimodal trend from the early morning.

The volume aerosol concentration of coarse mode ($c_{v,c}$), on the other hand, slowly increases throughout the day from 11:00 UTC, ranging from 0.6×10^{-6} cm^3/cm^2 to 1.2×10^{-6} cm^3/cm^2 after the onset of the SB. Also in this case, being the radius unvaried, the increase of the volume concentration is due to an increase of the number of particles simultaneous to the arrival of air mass from SB.

In Fig. 7, the aerosols volume size distribution is shown. In order to focus on the onset of the SB front and the breeze steady establishment, for all the investigated cases the volume size distribution of the aerosols refers to the period between 10:00 and 14:00 UTC. Before the development of the SB, the peak of the fine mode assumes the minima values of the day and remains almost constant (about 1×10^{-6} cm^3/cm^2) during the onset of the front (12:00–12:20 UTC). After the setting up of the SB, the atmospheric content of fine particles increases, reaching a maximum value of about 3×10^{-6} cm^3/cm^2 at 14:00 UTC, i.e. when the SB is steady. Then, it gradually decreases.

Differently, the total volume of coarse particles increases during the day reaching peaks of about 8.5×10^{-6} cm^3/cm^2 during the

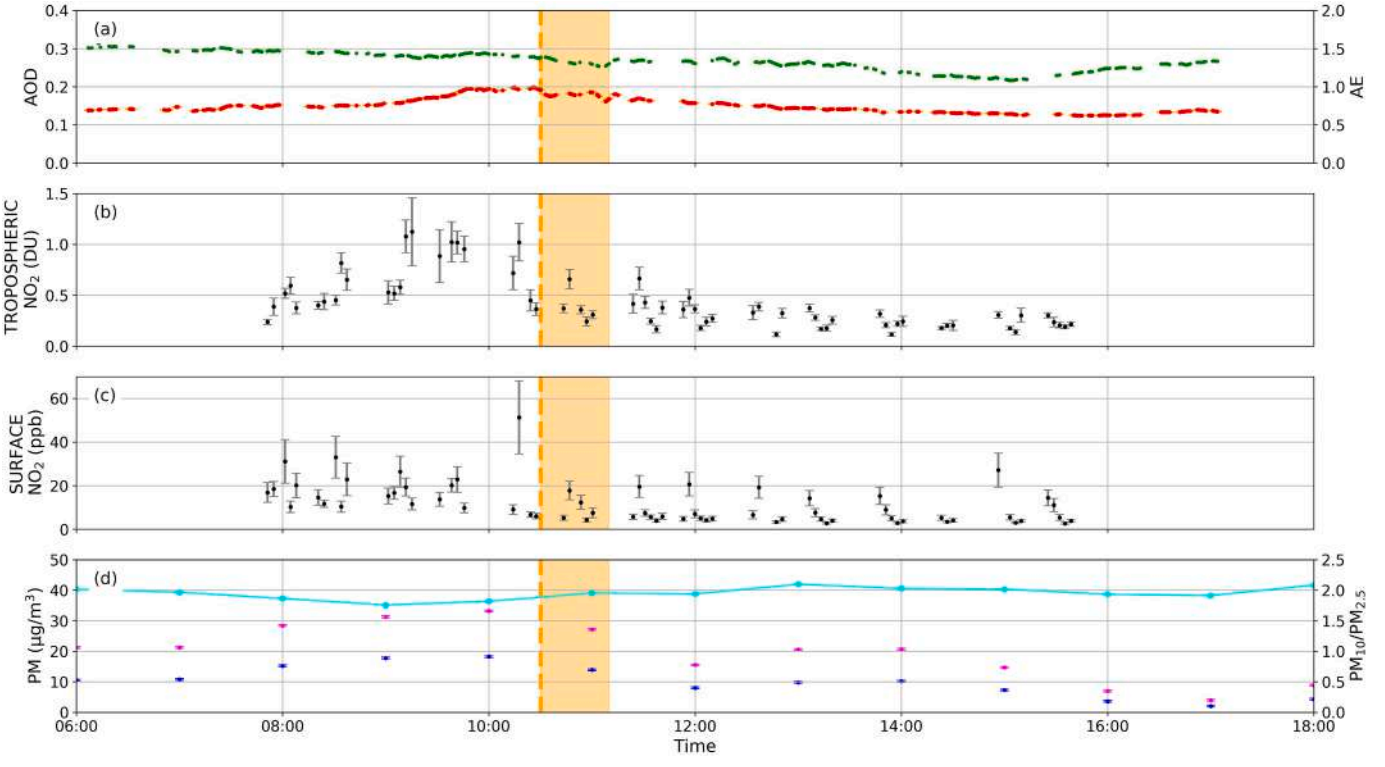

Fig. 8. Daily variation of (a) AOD (red dots) and AE (green dots), (b) tropospheric and (c) surface NO_2 amount, (d) PM_{10} (purple dots) and $PM_{2.5}$ (blue dots) concentration and $PM_{10}/PM_{2.5}$ ratio (cyan line) on 2 July 2019. The orange dashed line represents the arrival of the SB front. The orange-filled area depicts the time interval required for the complete development of the SB. (For interpretation of the references to colour in this figure legend, the reader is referred to the web version of this article.)

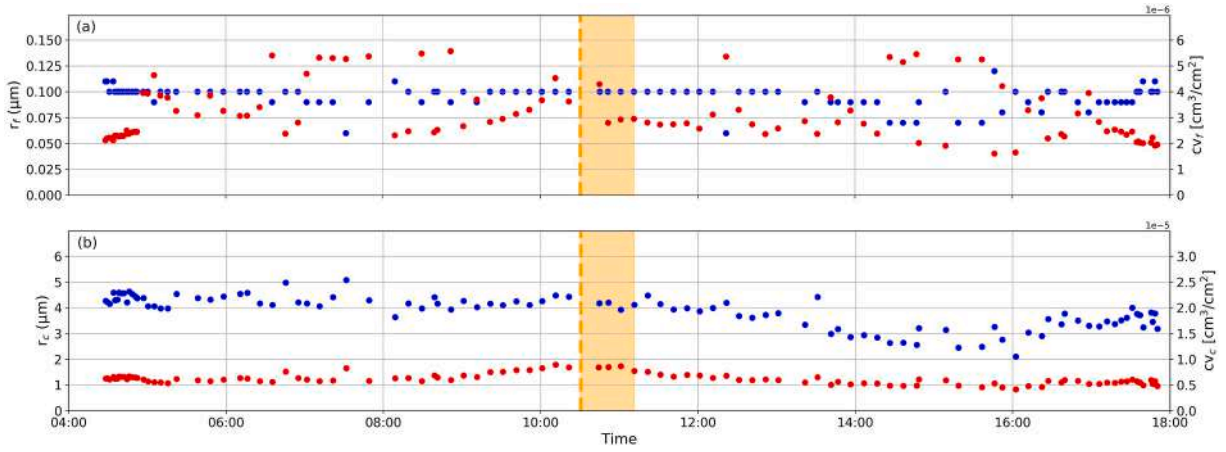

Fig. 9. Daily variation of modal radius (blue) and concentration values (red) for (a) fine aerosols and (b) coarse aerosols on 2 July 2019. The orange dashed line represents the arrival of the SB front. The orange-filled area depicts the time interval required for the complete development of the SB. (For interpretation of the references to colour in this figure legend, the reader is referred to the web version of this article.)

afternoon, approximately 3 times those of the fine mode. From the early morning, the volume size distribution follows a trimodal distribution with a double peak in the coarse mode. This behaviour is evident also after the establishment of the breeze regime and slowly fades out in the afternoon, when there is a considerable increase in the volume size distribution values of the coarse mode. Nevertheless, the passage of the SB front is clearly recognizable, as the distribution changes considerably with a sharp increase in both peak values of coarse mode (from 2×10^{-6} cm^3/cm^2 to 3×10^{-6} cm^3/cm^2 and from 3×10^{-6} cm^3/cm^2 to 4×10^{-6} cm^3/cm^2, respectively).

The coarse mode curves remain quite wide and continue to increase in peak values even after the steady establishment of SB and in the afternoon. On the contrary, after the SB development, the content of the accumulation mode decreases and settles on pre-front values. Unlike findings by Moorthy et al. (1993), during the passage of the SB front, the aerosol size distribution has not a clear bimodal trend. The difference, as previously highlighted, could be attributable to the presence of urban aerosol.

Front days results indicate that aerosol composition changes considerably with the arrival of the SB front: the fine mode shows a constant modal radius with an increase in concentration, proving that the number of fine particles, moved by the front, increases. At the same time, the almost constant coarse modal radius and the corresponding increases in volume suggest that the SB also carries coarse particles. The simultaneous and very clear increase of volume concentrations of both coarse and fine modes (44% and 23%, respectively) in a short temporal scale as the onset of the SB, very well discriminates the changes occurred in the atmosphere due to the SB air masses advection from those slowly happening in the time scale of several hours, due to the modulation of anthropogenic emissions inside the boundary layer. Nonetheless, the geographical position of the measurement site must be taken into account: before being investigated by the photometers, the air is transported by the SB front passing through a large portion of the city, mixing the sea aerosols with those produced locally in the urban environment. However, without an aerosol vertical profile, it is not possible identify where particles transported from SB are located.

4.2. Gentle breeze days

Fig. 8a shows the temporal variation of AOD and AE related to July 2, 2019, a day characterized by a "gentle" arrival of the breeze over the city. In agreement with the results by Moorthy et al. (1993), the slow development of the SB front does not cause a sharp modification of the optical characteristics of the aerosol. The AOD is constant during the morning and decreases progressively after a peak around 10:00 UTC (about 0.21). When the breeze onsets, i.e. at 10:30 UTC, the AOD continues to decrease following its previous trend and, in the afternoon, it assumes constant values (approximately 0.15), comparable to the morning ones. Even the AE is not particularly affected by the breeze: during the day, it decreases from 1.5 to 1.0, and then rises to 1.25. The arrival of the SB corresponds to a slight increase of AE, approximately from 1.25 to 1.30.

Fig. 8b and c show the trends of tropospheric and surface NO_2. Both tropospheric column and surface concentration decrease when the maximum solar radiation occurs, and no significant effects are noticed at the arrival of the SB. Surface NO_2 shows some values above the daily average but, as shown by error bars, these data have a large uncertainty. Therefore, they must be considered with a certain degree of caution.

Ground-based particulate matter concentration (Fig. 8d) has a similar trend in the case of front days and gentle breeze days. In fact, both PM_{10} and $PM_{2.5}$ concentrations strongly decrease before the onset of the SB and increase about one hour after its steady development. In this case, the concentration of PM_{10} increases more than $PM_{2.5}$, ranging from 16 $\mu g/m^3$ to 21 $\mu g/m^3$ and from 8 $\mu g/m^3$ to 10 $\mu g/m^3$, respectively. It follows that the $PM_{10}/PM_{2.5}$ ratio has a slight increase at 13:00 UTC and then remains almost constant.

In Fig. 9a and b, the temporal trends of fine and coarse aerosol components in the case of gentle breeze days are shown. The fine mode has no significant variations in r_f during the day. Only between 06:30 UTC and 09:00 UTC and from 13:00 UTC onwards, the fine

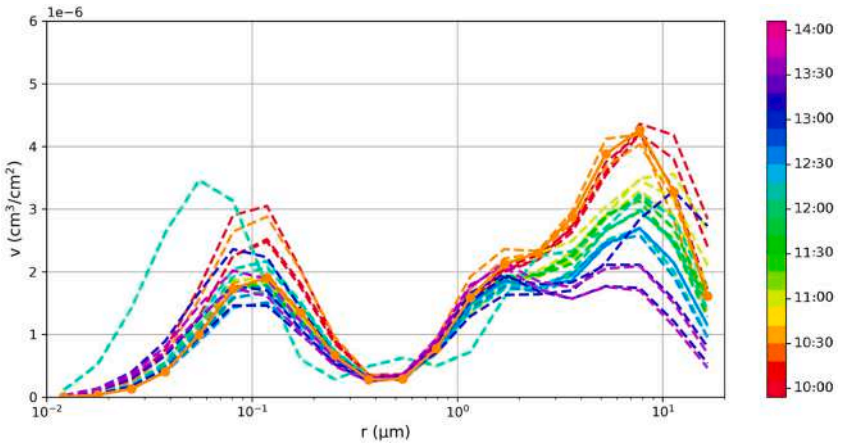

Fig. 10. Daily variation of volume size distribution on 2 July 2019 (from 10:00 up to 14:00 UTC). Marked line refers to the SB onset.

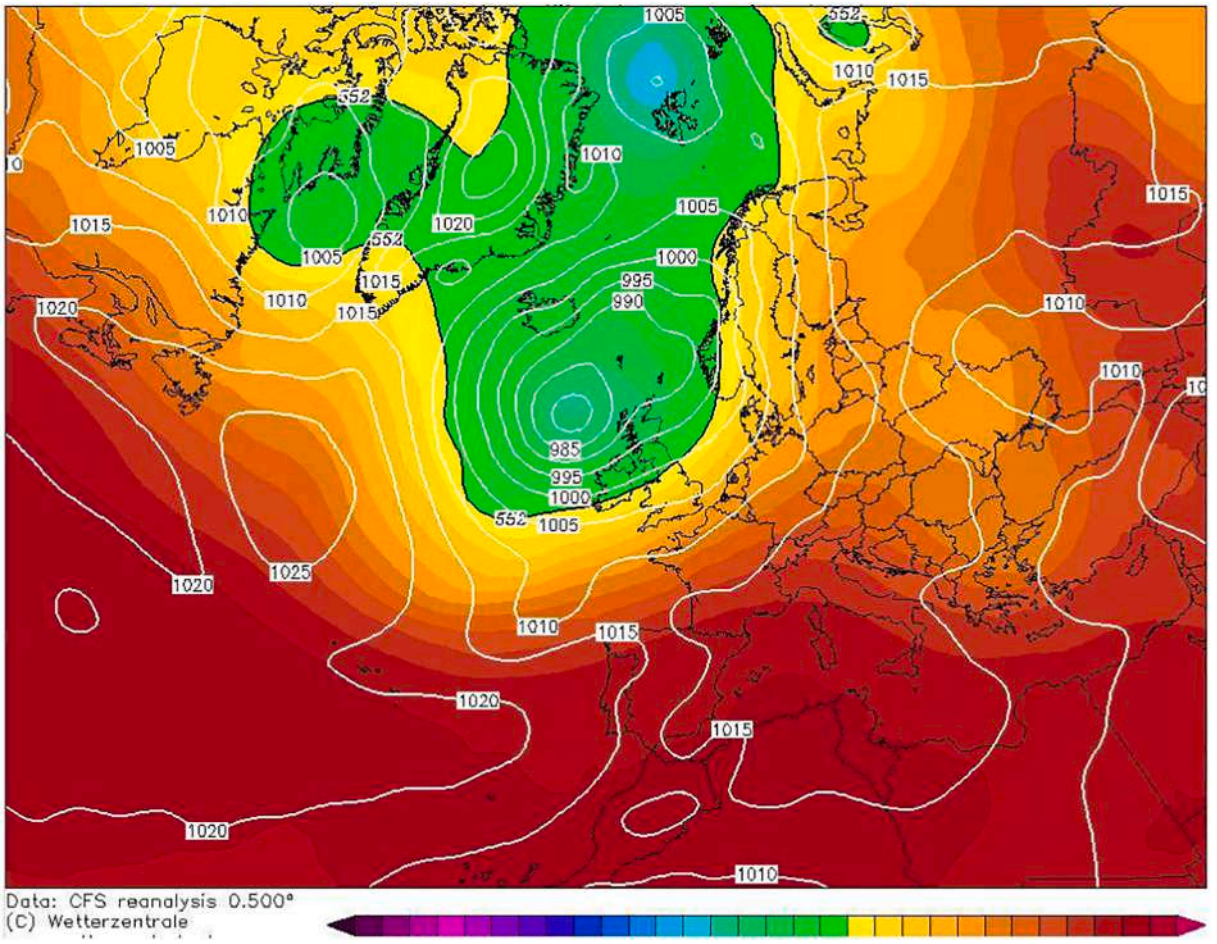

Fig. 11. Synoptic conditions on 17 August 2019 at 12:00 UTC from the Climate Forecast System (CFS) reanalysis. Colours refer to geopotential height at 500 hPa (in geopotential decametres). White contours are isobars (hPa) at sea level (source: https://www.wetterzentrale.de/).

modal radius ranges between 0.07 μm and 0.12 μm. Effects related to the breeze are not detectable. In the early morning, $c_{v,f}$ fluctuates between 2×10^{-6} cm^3/cm^2 and 6×10^{-6} cm^3/cm^2 with a sharp decrease (about 22%) during the gradual passage of the SB front (from 4.1×10^{-6} cm^3/cm^2 up to 3×10^{-6} cm^3/cm^2).

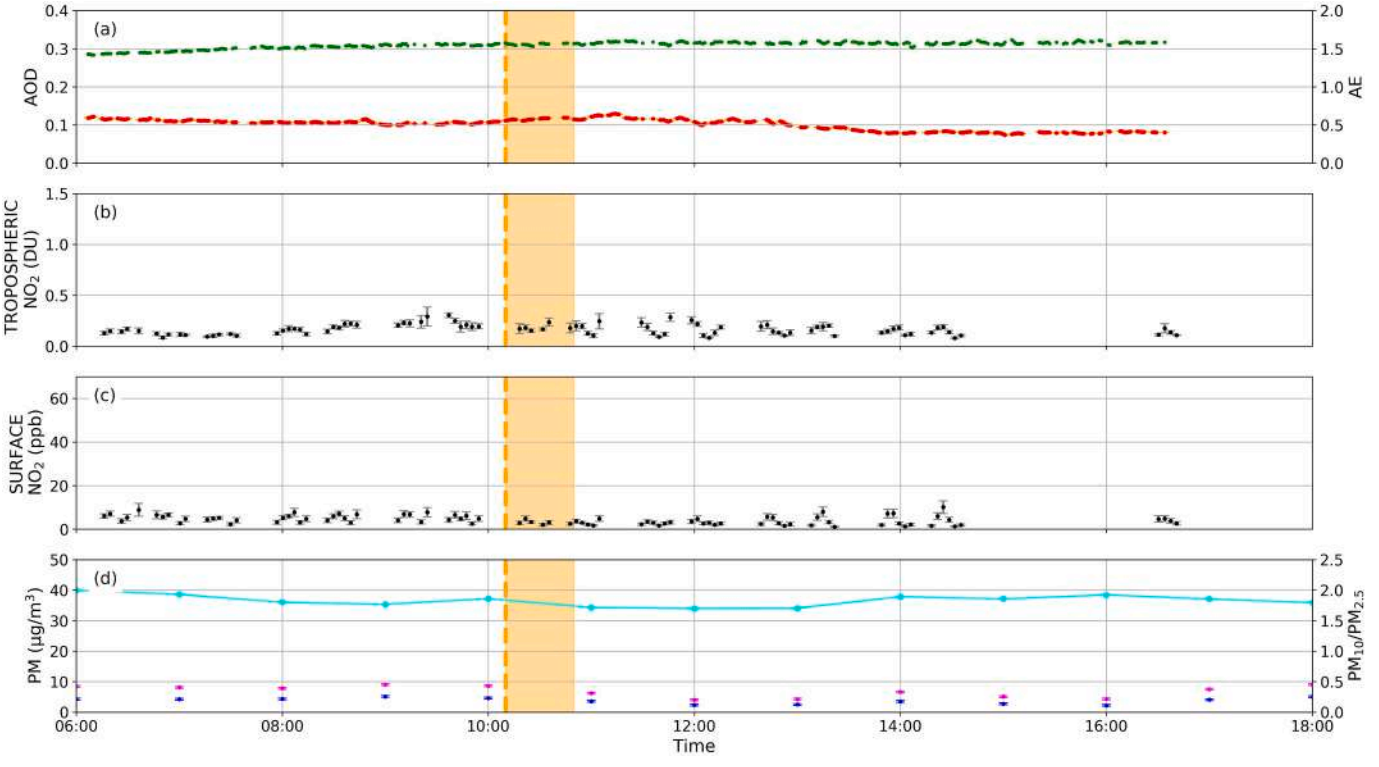

Fig. 12. Daily variation of (a) AOD (red dots) and AE (green dots), (b) tropospheric and (c) surface NO_2 amount, (d) PM_{10} (purple dots) and $PM_{2.5}$ (blue dots) concentration and $PM_{10}/PM_{2.5}$ ratio (cyan line) on 18 August 2019. The orange dashed line represents the arrival of the SB front. The orange-filled area depicts the time interval required for the complete development of the SB. (For interpretation of the references to colour in this figure legend, the reader is referred to the web version of this article.)

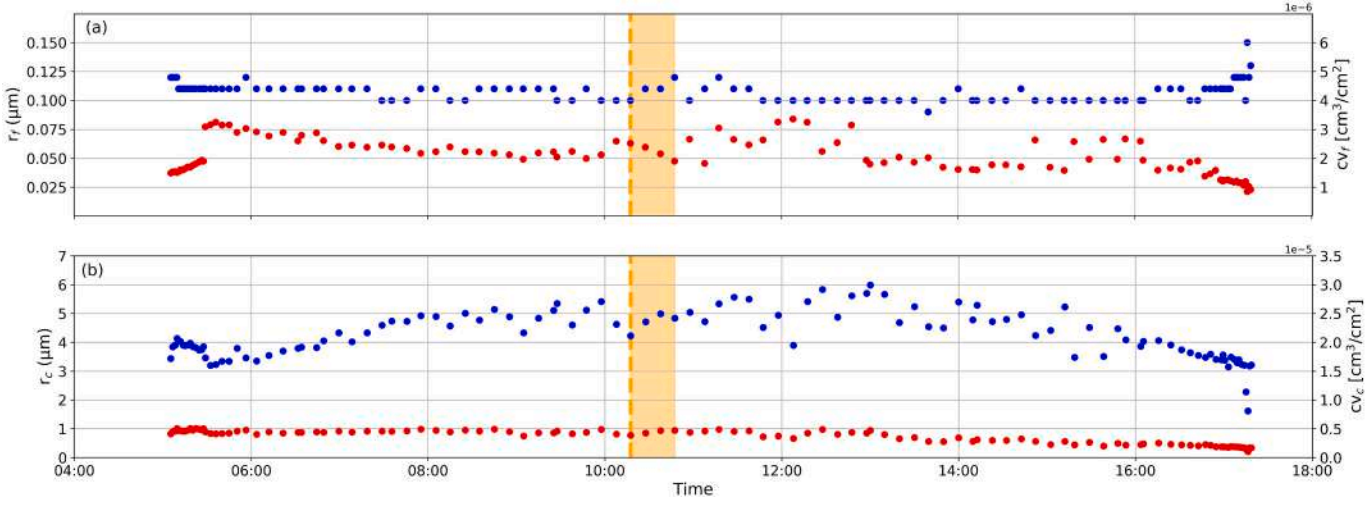

Fig. 13. Daily variation of modal radius (blue) and concentration values (red) for (a) fine aerosols and (b) coarse aerosols on 18 August 2019. The orange dashed line represents the arrival of the SB front. The orange-filled area depicts the time interval required for the complete development of the SB. (For interpretation of the references to colour in this figure legend, the reader is referred to the web version of this article.)

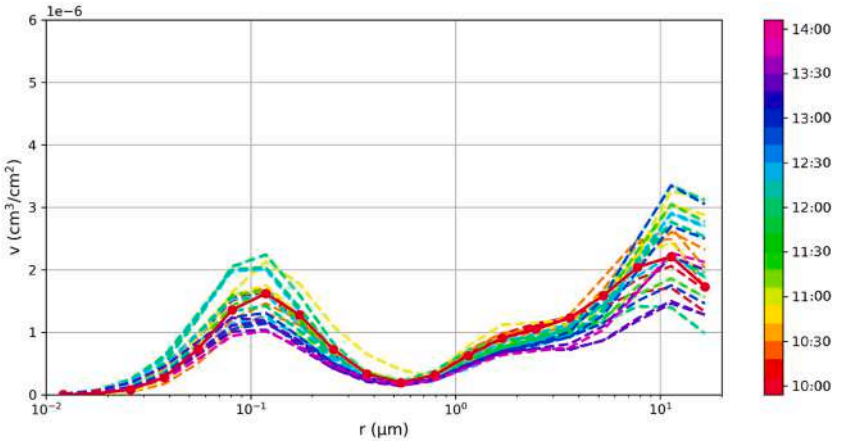

Fig. 14. Daily variation of volume size distribution on 18 August 2019 (from 10:00 up to 14:00 UTC). Marked line refers to the SB onset.

The daily trend of the coarse mode shows a slight decrease of $c_{v,c}$ (around 9%) at the turn of the SB front and almost constant values of $c_{v,c}$ throughout the day.

The volume size distribution of the aerosol (Fig. 10) shows a clear bimodal behaviour only before the SB onset. Furthermore, the curve of coarse mode shows a peak value of about 4.1×10^{-6} cm^3/cm^2 at 11:00 UTC with a content comparable to the fine mode (peak of about 3.1×10^{-6} cm^3/cm^2), unlike what presented in Fig. 7, where the contribution of coarse mode was sharply predominant. Unfortunately, since the vertical profiles of the aerosols are not available, we have no information about the particles position and we cannot know if the day of 2 July 2019 was characterized by a different "background" aerosol content compared to that of 1 August 2019, previously analysed. Nonetheless, in gentle breeze days, it can be assumed that the breeze changes the aerosol content, which increases during the morning and the SB front development and decrease considerably when the breeze is steady (i.e. from 11:10 UTC). In fact, the peak value of the coarse mode increases in the hours preceding the arrival of the front, ranging from 2.5×10^{-6} cm^3/cm^2 to 3.4×10^{-6} cm^3/cm^2 and it does not vary significantly during the breeze development. After the onset of SB, the volumetric contribution of the fine aerosol decreases progressively (except for a temporary increase at 12:30 UTC) returning to the pre-front values. The peak of the coarse mode occurs at 11:00 UTC (4.1×10^{-6} cm^3/cm^2) and decreases considerably from 11:30 UTC, i.e. after the onset of the breeze.

Unlike the SB front days, in gentle breeze days the development of the SB causes a net change in the volume size distribution: the content of fine aerosol has a slight decrease while the amount of coarse mode particles decreases considerably. The above-described observations suggest that, in the case of gentle breeze days, the air carried by the breeze in the absence of a well-defined front does not contain a high concentration of fine-mode aerosols. Nevertheless, it is not possible to discern with certainty the aerosol component due to the advection of the SB front from the local emissions, because, as stated, the background situation of the front day and the gentle breeze day analysed are not known.

Several gentle breeze days occur when large-scale weather conditions prevail over local phenomena for at least 48 h. These events are characterized by typically moderate wind speed and nearly constant direction. In fact, the synoptic scale circulation governs the local weather and, only in the summer months, when also the SB can develop easily, the synoptic effects are added to those of the local breeze regime.

For instance, from 12 to 17 August 2019, a persistent, low-pressure centre was located north of Great Britain, while a high-pressure centre was located over Italy and the Mediterranean basin (Fig. 11). These weather conditions determine, over the central region of Italy, the prevalence of synoptic wind blowing from the West and North-West sectors. In what follows, results refer to the 18th of August 2019. Starting from August 14, 2019, the wind blows mainly from the western sector, with daily average daily speeds between 1.5 and 1.9 m/s and more intense wind speeds during daytime, when the sea breeze is added to the synoptic effect. During the day, the ground-based weather station recorded wind gusts with velocities up to 9.5 m/s.

In these cases, the onset of SB does not change significantly the optical properties of aerosols and NO_2 amounts (Figs. 12 and 13), which remain constant throughout the day. In fact, because of the prevalence of synoptic wind, aerosols and particulate matters present in the lower layer of the atmosphere are well-mixed and also the accumulation of marine aerosol that typically occurs during nighttime and in the early morning in the atmosphere above the surface of the sea thanks to the low-speed mesoscale circulation (as the land breeze, among others), does not occur. It follows that the SB does not advect cooler and moister air compared to the urban one and, therefore, the SB front is not well detectable.

AOD and AE (Fig. 12a) have constant values throughout the day. In particular, the AOD fluctuates between 0.11 and 0.14 until 13:00 UTC and, then, slowly decreases until it reaches 0.08 in the late afternoon. Upon arrival of the breeze (up to 11:10 UTC), the AOD increases slightly (approximately 5%) and then continues its decreasing trend. The AE increases in the early morning hours from 1.3 to 1.5 and remains constant during the breeze hours. No changes take place at the SB onset.

Unlike the cases previously analysed, tropospheric and surface NO_2 (Fig. 12b and c) do not vary during the day. In fact, except for a slight increase in tropospheric NO_2 at about 9:30 UTC, concentrations remain constant throughout the day. This is mainly due to the

effect of the strong synoptic wind, which, in previous days, removed most of the urban pollution reducing the background values. The effect is also noticeable on the ground: both surface NO_2 and PM (Fig. 15d) assume very low values with respect to the aforementioned cases. Surface NO_2 rarely exceeds 5 ppb during the day, while PM_{10} and $PM_{2.5}$ are always below 10 μg. On the other hand, it is important to underline that the low concentrations of PMs and NO_2 could be related to the investigated day: mid-August, in Italy, typically coincides with the main summer holiday period, when anthropogenic emissions are strongly reduced due to the work activity suspension and traffic is at its yearly minimum. As in the other cases, the PM concentration increases after one hour from the development of the breeze, although modestly. The $PM_{10}/PM_{2.5}$ ratio value remains constant, showing that the particulate composition does not vary with the development of the breeze.

During the development period of the SB front, the radius of the fine aerosols (Fig. 13a) on 18 August 2019 increases from 0.1 μm to 0.125 μm, decreasing again an hour after the establishment of the SB regime until the morning values. The volumetric content $c_{v,f}$ increases with the passage of the breeze front of about 3% and ranges between 2×10^{-6} cm^3/cm^2 and 3.5×10^{-6} cm^3/cm^2 until 13:00 UTC. Then, it settles on 2×10^{-6} cm^3/cm^2. This means that, when the SB in developed, there are larger particles in the atmosphere but fewer in number than in the pre-front situation. When the breeze regime is well established, the modal radius of the fine mode fluctuates and the volumetric content increases. This suggests that the atmospheric aerosol particles have increased in number but are slightly larger than those present before the onset of the breeze. The aerosol coarse mode (Fig. 13b), on the other hand, increases in radius in the early hours of the morning, oscillating during the day between 4 μm and 6 μm. At the turn of the SB front, $c_{v,f}$ decreases of approximatively 5% and, upon the arrival of the breeze front and r_c increases, while the value of the volumetric content $c_{v,c}$ remains constant. Hence, the number of coarse particles decreases. This confirms that the SB front carries primarily fine particles.

The temporal evolution of the volume size distribution is given in Fig. 14 and shows that, also in this case, the aerosol volume distribution is clearly trimodal after the establishment of the breeze (i.e. from 10:10 UTC) with two peaks in the coarse mode. The fine-mode content decreases before the arrival of the SB (peak from 1.9×10^{-6} cm^3/cm^2 to 1.4×10^{-6} cm^3/cm^2). During the passage of the front, the peak value remains constant (about 1.4×10^{-6} cm^3/cm^2) and immediately afterwards it decreases down to 1.3×10^{-6} cm^3/cm^2. Referring to the coarse mode, the radius equal to about 11.3 μm assumes the highest values throughout the day, with peaks of 3.3×10^{-6} cm^3/cm^2 at 11:20 UTC and at 12:20 UTC. As for the fine mode, also the volumetric distribution of the coarse mode decreases immediately after the passage of the SB front and increases again from 11:00 UTC.

The results show that the passage of the breeze front determines an increase in the number and size of fine particles and a reduction in the number of coarse particles. However, in this configuration, as for the particulate matter and for NO_2, the aerosol content is lower than the other cases. Again, it is important to point out that the period analysed in this case coincides with the typical annual minimum of local anthropogenic emissions due to the summer holidays.

5. Conclusions

In this paper, several ground-based remote sensing and in situ instruments have been used to analyse in detail the effect of the sea breeze circulation on aerosol properties in the urban area of Rome, Italy.

The criteria chosen for the identification and the classification of the SB front consider several meteorological variables: (i) clear days with high-pressure systems, with no rainfall recorded in the time window relevant to the sea-breeze passage; (ii) change in surface wind direction and wind intensity some hours after sunrise, with the wind blowing from the sea to the land, perpendicularly to the coastline; (iii) increase in specific humidity and content of total column water vapour, associated with a simultaneous decrease in the atmospheric temperature because of cooler, moister air coming from the sea.

Based on the time interval required for the development of the SB front, two characteristic patterns, found frequently during the summer months in the Rome area, have been identified:

a) “front breeze day”, in which the SB front is well detectable thanks to the sharp change of surface meteorological quantities, which pass from the pre-front values to those typical of the sea breeze in a few minutes (less than 20 min);
b) “gentle breeze day”, characterized by a gradual or “gentle” onset of the SB (about 1 h), without a net increase in atmospheric total column water vapour and specific humidity and decrease of surface air temperature.

Although the area under examination is exposed to the breeze regime during the whole year, the months of June, July and August 2018 and 2019 were considered in the present study. The analysis of the meteorological conditions allowed the identification of 48 days that meet the criteria listed above. Of these, 40% belong to the front days while, in 60% of cases, the breeze followed the evolution corresponding to the gentle breeze days.

In both cases, the advection of cooler and moister air changes the physical and optical characteristics of the aerosols.

In front breeze cases, a net increase in AOD is detectable at the turn of the SB front, while the AE is not significantly affected by the arrival of the breeze. The change in NO_2 tropospheric columns and surface concentrations is not appreciable during the onset of the SB, even if the effect of the local sources is not identifiable. Ground-based measurements of PM_{10} and $PM_{2.5}$ show a simultaneous decrease in concentration before the SB onset while, after the development of the breeze, both components show a net increase. Consequently, the relative composition of the particulate matter is not affected by the passage of the breeze front. The volume size distribution shows a trimodal trend during the day, with two peaks in the coarse mode. As the breeze front develops, both the fine and the coarse modal radii remain fairly constant. On the other hand, a remarkable increase both in the fine (+44%) and coarse (+23%) volumetric contents have been found. These observations suggest that the SB front carries over the city a considerable component of fine particles. However, since the vertical aerosol profiles are not available, it is not possible to differentiate the contribution from local sources from

Table 3
Effect of SB development on optical and physical properties of aerosols and gases at the turn of the SB front.

Parameter	Front day	Gentle breeze days
AOD	Net increase	Not affected
AE	Not appreciable	Not appreciable
PM_{10}	Decrease before the SB onset, then net increase	Decrease before the SB onset, then net increase
$PM_{2.5}$	Decrease before the SB onset, then net increase	Decrease before the SB onset, then net increase
$PM_{10}/PM_{2.5}$	Not appreciable	Slight increase
r_f	Not appreciable	Not appreciable
$c_{v,f}$	Net increase	Net decrease
r_c	Not appreciable	Not appreciable
$c_{v,c}$	Net increase	Slight decrease
Volume size distribution	Trimodal trend	Bimodal trend before the sb onset, then trimodal
NO_2 tropospheric	Not appreciable	Not appreciable
NO_2 near-surface	Not appreciable	Not appreciable

the one due to the sea breeze.

During the gentle breeze days, AOD, AE, tropospheric NO_2 columns, and surface NO_2 are not considerably affected by the arrival of the SB. PM_{10} and $PM_{2.5}$ concentrations show a similar trend in the case of front days and gentle breeze days, while the $PM_{10}/PM_{2.5}$ ratio has a slight increase with the gradual onset of the breeze. The aerosol volume size distribution has a bimodal distribution only before the breeze onset. Both the fine and coarse modal radii are almost constant during the gradual SB onset while the volumetric content decreases of about 22% and 9% for fine and coarse mode, respectively.

It should be noted that sometimes the development of gentle breezes occurs following the establishment of at least 48 h of perturbations due to prevailing geostrophic wind. In this case, the air carried by the breeze over the city is not particularly cooler and moister and has a lower aerosol load. During these days, the breeze has no significant effects on the optical properties of aerosols and gases.

The effect of the two breeze patterns on the optical and physical properties of the aerosols and gases examined are summarized in Table 3.

The interaction between mesoscale and local circulation makes the analysis of SB a difficult task, especially in conditions of complex orography and presence of an anthropized environment. For this reason, in-situ data with high quality and high temporal resolution are fundamental. The analysis would certainly be completed considering the vertical profiles of the aerosols, which can provide rigorous information on the temporal development of the TIBL and on the quote of the aerosols.

Future studies may concern the speciation of aerosols and their vertical distribution in order to characterize air masses origins and aerosol types. Furthermore, possible future developments concern the detailed investigation of the temporal evolution of the SB front, using e.g. data from urban LIDARs and ceilometers.

Further analysis will also be dedicated to the investigation of the interaction between the onset of the SB and the photochemical reactions, typical of NO_2 in urban environments. In fact, although this topic is of great interest for the scientific community, it is not well known how the breeze front and the TIBL modifies the surface and columnar loads of NO_2.

Moreover, it would be interesting to analyse how the breeze front moves from the coastline to the urban inland, using meteorological and air quality data, also from suburban and coastal stations operating in the Rome area. This would allow the exhaustive study of the SB front, including its development, and verify if the differences between the front days and gentle breeze days are also evident in the coastal region or derive from the interaction with the urban environment. Additionally, it would be interesting to use meteorological or atmospheric transport models to interpret the development of the SB front and its interaction with gases and aerosols present in the urban environment. The discussion of this topic will be dealt with in a future dedicated paper. Furthermore, the presented results might be a useful tool also for a correct modelling of SB events: knowing when and how the SB develops can provide advantageous information for a successful prediction of local scale circulation and air quality trend.

Declaration of Competing Interest

The authors declare that they have no known competing financial interests or personal relationships that could have appeared to influence the work reported in this paper.

Acknowledgements

The authors gratefully acknowledge ARPA Lazio for providing particulate matter measurements, Meteo Lazio and Fondazione Osservatorio Milano Duomo for the required meteorological used in this publication. The Pandonia Global Network (PGN) is a bilateral project supported with funding from NASA and ESA. This research was supported by BAQUNIN Project team, funded by ESA through the contract ID 4000126749/19/I-NS, the BAQUNIN team provided insight and expertise that greatly assisted the research.

References

Ahrens, C.D., 2012. Meteorology Today: An Introduction to Weather, Climate, and the Environment. Cengage Learning.

Atkins, N.T., Wakimoto, R.M., Weckwerth, T.M., 1995. Observations of the sea-breeze front during CaPE. Part II: dual-Doppler and aircraft analysis. Mon. Weather Rev. 123 (4), 944–969. https://doi.org/10.1175/1520-0493(1995)123<0944:OOTSBF>2.0.CO;2.

Augustin, P., Billet, S., Crumeyrolle, S., Deboudt, K., Dieudonné, E., Flament, P., Fourmentin, M., Guilbaud, S., Hanoune, B., Landkocz, Y., Méausoone, C., Roy, S., Schmitt, F., Sentchev, A., Sokolov, A., 2020. Impact of sea breeze dynamics on atmospheric pollutants and their toxicity in industrial and urban coastal environments. Remote Sens. 12 (4), 648. https://doi.org/10.3390/rs12040648.

Azorin-Molina, C., Tijm, S., Chen, D., 2011. Development of selection algorithms and databases for sea breeze studies. Theor. Appl. Climatol. 106 (3–4), 531–546. https://doi.org/10.1007/s00704-011-0454-4.

Azouzoute, A., Merrouni, A.A., Gennioui, A., 2019. Accuracy measurement of Pyranometer vs reference cell for PV resource assessment. Energy Procedia 157 (1202–1209), 1202–1209. https://doi.org/10.1016/j.egypro.2018.11.286.

Beirle, S., Platt, U., Wenig, M., Wagner, T., 2003. Weekly Cycle of NO2 by GOME Measurements: A Signature of Anthropogenic Sources.

Beirle, S., Boersma, K.F., Platt, U., Lawrence, M.G., Wagner, T., 2011. Megacity emissions and lifetimes of nitrogen oxides probed from space. Science 333 (6050), 1737–1739. https://doi.org/10.1126/science.1207824.

Boyouk, N., Léon, J.F., Delbarre, H., Augustin, P., Fourmentin, M., 2011. Impact of sea breeze on vertical structure of aerosol optical properties in Dunkerque, France. Atmos. Res. 101 (4), 902–910. https://doi.org/10.1016/j.atmosres.2011.05.016.

Cafaro, C., Frame, T.H., Methven, J., Roberts, N., Bröcker, J., 2019. The added value of convection-permitting ensemble forecasts of sea breeze compared to a Bayesian forecast driven by the global ensemble. Q. J. R. Meteorol. Soc. 145 (721), 1780–1798. https://doi.org/10.1002/qj.3531.

Campanelli, M., Estellés, V., Tomasi, C., Nakajima, T., Malvestuto, V., Martínez-Lozano, J.A., 2007. Application of the SKYRAD improved Langley plot method for the in situ calibration of CIMEL sun-sky photometers. Appl. Opt. 46 (14), 2688–2702. https://doi.org/10.1364/AO.46.002688.

Campanelli, M., Estelles, V., Smyth, T., Tomasi, C., Martìnez-Lozano, M.P., Claxton, B., Muller, P., Pappalardo, G., Pietruczuk, A., Shanklin, J., Colwell, S., Wrench, C., Lupi, A., Mazzola, M., Lanconelli, C., Vitale, V., Congeduti, F., Dionisi, D., Cardillo, F., Cacciani, M., Casasanta, G., Nakajima, T., 2012. Monitoring of Eyjafjallajökull volcanic aerosol by the new European Skynet Radiometers (ESR) network. Atmos. Environ. 48, 33–45. https://doi.org/10.1016/j.atmosenv.2011.09.070.

Casasanta, G., Di Bernardino, A., Iannarelli, A.M., Casadio, S., Petenko, I., Argentini, S., Mevi, G., Cacciani, M., 2021. Estimating the accuracy in vertical wind speed determination with Doppler SODAR (in preparation).

Cede, A., 2019. Manual for Blick Software Suite 1.7. LuftBlick.

Cede, A., Tiefengraber, M., Gebetsberger, M., Kreuter, A., 2019. Fiducial Reference Measurements for Air Quality, LuftBlick Report 201909. LuftBlick.

Cenedese, A., Miozzi, M., Monti, P., 2000. A laboratory investigation of land and sea breeze regimes. Exp. Fluids 29 (1), S291–S299. https://doi.org/10.1007/s003480070031.

Charlson, R.J., Horvath, H., Pueschel, R.F., 1967. The direct measurement of atmospheric light scattering coefficient for studies of visibility and pollution. Atmos. Environ. 1 (4), 469–478. https://doi.org/10.1016/0004-6981(67)90062-5.

Colacino, M., 1982. Observations of a sea breeze event in the Rome area. Arch. Meteor. Geophys. Bioclim. Ser. B 30 (1–2), 127–139. https://doi.org/10.1007/BF02323399.

Cros, B., Durand, P., Cachier, H., Drobinski, P., Frejafon, E., Kottmeier, C., Perros, P.E., Peuch, V.-H., Ponche, J.-L., Robin, D., Saıd, F., Toupance, G., Wortham, H., 2004. The ESCOMPTE program: an overview. Atmos. Res. 69 (3–4), 241–279. https://doi.org/10.1016/j.atmosres.2003.05.001.

Crumeyrolle, S., Manninen, H.E., Sellegri, K., Roberts, G., Gomes, L., Kulmala, M., Weigel, R., Laj, P., Schwarzenboeck, A., 2010. New particle formation events measured on board the ATR-42 aircraft during the EUCAARI campaign. Atmos. Chem. Phys. 10, 6721–6735. https://doi.org/10.5194/acp-10-6721-2010.

Di Sarra, A., Cacciani, M., Chamard, P., Cornwall, C., DeLuisi, J.J., Di Iorio, T., Disterhoft, P., Fiocco, G., Fuà, D., Monteleone, F., 2002. Effects of desert dust and ozone on the ultraviolet irradiance at the Mediterranean island of Lampedusa during PAUR II. J. Geophys. Res.-Atmos. 107 (D18) https://doi.org/10.1029/2000JD000139. PAU-2.

Drosoglou, T., Bais, A.F., Zyrichidou, I., Kouremeti, N., Poupkou, A., Liora, N., Giannaros, C., Koukouli, M.E., Balis, D., Melas, D., 2017. Comparisons of ground-based tropospheric NO2 MAX-DOAS measurements to satellite observations with the aid of an air quality model over the Thessaloniki area, Greece. Atmos. Chem. Phys. 17 (9), 5829. https://doi.org/10.5194/acp-17-5829-2017.

Drosoglou, T., Koukouli, M.E., Kouremeti, N., Bais, A.F., Zyrichidou, I., Balis, D., Xu, J., Li, A., 2018. MAX-DOAS NO2 observations over Guangzhou, China; ground-based and satellite comparisons. Atmos. Measure. Techniques 11 (4), 2239–2255. https://doi.org/10.5194/amt-11-2239-2018.

Easter, R.C., Peters, L.K., 1994. Binary homogeneous nucleation: temperature and relative humidity fluctuations, nonlinearity, and aspects of new particle production in the atmosphere. J. Appl. Meteorol. 33 (7), 775–784. https://doi.org/10.1175/1520-0450(1994)033<0775:BHNTAR>2.0.CO;2.

Estellés, V., Campanelli, M., Smyth, T.J., Utrillas, M.P., Martínez-Lozano, J.A., 2012. AERONET and ESR sun direct products comparison performed on Cimel CE318 and Prede POM01 solar radiometers. Atmos. Chem. Phys. Dis. 12 (2) https://doi.org/10.5194/acpd-12-4341-2012.

Ferdiansyah, M.R., Inagaki, A., Kanda, M., 2020. Detection of sea-breeze inland penetration in the coastal-urban region using geostationary satellite images. Urban Clim. 31, 100586. https://doi.org/10.1016/j.uclim.2020.100586.

Ferretti, R., Mastrantonio, G., Argentini, S., Santoleri, R., Viola, A., 2003. A model-aided investigation of winter thermally driven circulation on the Italian Tyrrhenian coast: A case study. J. Geophys. Res.-Atmos. 108 (D24) https://doi.org/10.1029/2003JD003424.

Gahmberg, M., Savijärvi, H., Leskinen, M., 2010. The influence of synoptic scale flow on sea breeze induced surface winds and calm zones. Tellus A Dynamic Meteorol. Oceanogr. 62 (2), 209–217. https://doi.org/10.1111/j.1600-0870.2009.00423.x.

Giles, D.M., Sinyuk, A., Sorokin, M.S., Schafer, J.S., Smirnov, A., Slutsker, I., Eck, T.F., Holben, B.N., Lewis, J., Campbell, J., Welton, E.J., Korkin, S., Lyapustin, A. (2019). Advancements in the Aerosol Robotic Network (AERONET) Version 3 database–automated near-real-time quality control algorithm with improved cloud screening for Sun photometer aerosol optical depth (AOD) measurements. Atmos. Measure. Techniques, 12(1). DOI: https://doi.org/10.5194/amt-12-169-2019.

Gkikas, G., Barkoula, N.M., Paipetis, A.S., 2012. Effect of dispersion conditions on the thermo-mechanical and toughness properties of multi walled carbon nanotubes-reinforced epoxy. Compos. Part B 43 (6), 2697–2705. https://doi.org/10.1016/j.compositesb.2012.01.070.

Hunt, J.C.R., Simpson, J.E., 1982. Atmospheric boundary layers over non-homogeneous terrain. In: Plate, E. (Ed.), Chapter 7 of 'Engineering Meteorology'. Elsevier, pp. 269–318.

Iannarelli, A.M., Di Bernardino, A., Casadio, S., Bassani, C., Cacciani, C., Campanelli, M., Casasanta, G., Cadau, E., Diémoz, H., Mevi, G., Siani, A.M., Cardaci, M., Goril, P., Dehn, A., 2021. The challenging capability of BAQUNIN supersite for atmospheric observations in urban environment (in preparation).

Ito, T., 1993. Size distribution of Antarctic submicron aerosols. Tellus Ser. B Chem. Phys. Meteorol. 45 (2), 145–159. https://doi.org/10.3402/tellusb.v45i2.15589.

Macias, E.S., Husar, R.B., 1976. Atmospheric particulate mass measurement with Beta attenuation mass monitor. Environ. Sci. Technol. 10, 904–907. https://doi.org/10.1021/es60120a015.

Mastrantonio, G., Fiocco, G., 1982. Accuracy of wind velocity determinations with Doppler sodars. J. Appl. Meteorol. 21 (6), 823–830. https://doi.org/10.1175/1520-0450(1982)021<0823:AOWVDW>2.0.CO;2.

Mastrantonio, G., Argentini, S., Viola, A., 1994. A new PC-based real time system to analyze Sodar-echoes. Ital. Res. Antarctic Atmos. Ital. Phys. Soc. Bologna 45, 227–235.

Mavroidis, I., Chaloulakou, A., 2011. Long-term trends of primary and secondary NO2 production in the Athens area. Variation of the NO2/NOx ratio. Atmos. Environ. 45 (38), 6872–6879. https://doi.org/10.1016/j.atmosenv.2010.11.006.

Melas, D., Ziomas, I.C., Zerefos, C.S., 1995. Boundary layer dynamics in an urban coastal environment under sea breeze conditions. Atmos. Environ. 29 (24), 3605–3617. https://doi.org/10.1016/1352-2310(95)00140-T.

Meloni, D., Di Sarra, A., Biavati, G., DeLuisi, J.J., Monteleone, F., Pace, G., Piacentino, S., Sferlazzo, D.M., 2007. Seasonal behavior of Saharan dust events at the Mediterranean island of Lampedusa in the period 1999–2005. Atmos. Environ. 41 (14), 3041–3056. https://doi.org/10.1016/j.atmosenv.2006.12.001.

Meszaros, E., 1968. On the size distribution of water-soluble particles in the atmosphere. Tellus 20 (3), 443–448. https://doi.org/10.1111/j.2153-3490.1968.tb00385.x.

Miller, S.T.K., Keim, B.D., Talbot, R.W., Mao, H., 2003. Sea breeze: structure, forecasting, and impacts. Rev. Geophys. 41 (3) https://doi.org/10.1029/2003RG000124.

Mitsumoto, S., Ueda, H., Ozoe, H., 1983. A laboratory experiment on the dynamics of the land and sea breeze. J. Atmos. Sci. 40 (5), 1228–1240. https://doi.org/10.1175/1520-0469(1983)040<1228:ALEOTD>2.0.CO;2.

Monti, P., Leuzzi, G., 2005. A numerical study of mesoscale airflow and dispersion over coastal complex terrain. Int. J. Environ. Pollut. 25 (1), 239–250. https://doi.org/10.1504/IJEP.2005.007670.

Moorthy, K.K., Murthy, B.K., Nair, P.R., 1993. Sea-breeze front effects on boundary-layer aerosols at a tropical coastal station. J. Appl. Meteorol. 32 (7), 1196–1205. https://doi.org/10.1175/1520-0450(1993)032<1196:SBFEOB>2.0.CO;2.

Moorthy, K.K., Pillai, P.S., Babu, S.S., 2003. Influence of changes in the prevailing synoptic conditions on the response of aerosol characteristics to land-and sea-breeze circulations at a coastal station. Bound.-Layer Meteorol. 108 (1), 145–161. https://doi.org/10.1023/A:1023073929115.

Nakajima, T., Campanelli, M., Che, H., Estellés, V., Irie, H., Kim, S.W., Kim, J., Liu, D., Nishizawa, T., Pandithurai, G., Soni, V.K., Thana, B., Tugjsurn, N.U., Aoki, K., Go, S., Hashimoto, M., Higurashi, A., Kazadzis, S., Khatri, P., Kouremeti, N., Kudo, R., Marenco, F., Momoi, M., Ningombam, S.S., Ryder, C.L., Uchiyama, A., Yamazaki, A., 2020. An overview of and issues with sky radiometer technology and SKYNET. Atmos. Measure. Techniques 13 (8), 4195–4218. https://doi.org/10.5194/amt-13-4195-2020.

Pelliccioni, A., Monti, P., Leuzzi, G., 2015. An alternative wind profile formulation for urban areas in neutral conditions. Environ. Fluid Mech. 15 (1), 135–146. https://doi.org/10.1007/s10652-014-9364-1.

Pelliccioni, A., Monti, P., Cattani, G., Boccuni, F., Cacciani, M., Canepari, S., Capone, P., Catrambone, M., Cusano, M., D'Ovidio, M.C., De Santis, A., Di Bernardino, A., Di Menno di Bucchianico, A., Di Renzi, S., Ferrante, R., Gaeta, A., Gaddi, R., Gherardi, M., Giusto, M., Gordiani, A., Grandoni, L., Leone, G., Leuzzi, G., L'Episcopo, N., Marcovecchio, F., Pini, A., Sargolini, T., Tombolini, F., Tofful, L., Perrino, C., 2020. Integrated evaluation of indoor particulate exposure: the viepi project. Sustainability 12 (22), 9758. https://doi.org/10.3390/su12229758.

Pérez-Ramírez, D., Whiteman, D.N., Smirnov, A., Lyamani, H., Holben, B.N., Pinker, R., Andrarde, M., Alados-Arboledas, L., 2014. Evaluation of AERONET precipitable water vapor versus microwave radiometry, GPS, and radiosondes at ARM sites. J. Geophys. Res.: Atmos. 119 (15), 9596–9613. https://doi.org/10.1002/2014JD021730.

Petenko, I., Mastrantonio, G., Viola, A., Argentini, S., Coniglio, L., Monti, P., Leuzzi, G., 2011. Local circulation diurnal patterns and their relationship with large-scale flows in a coastal area of the Tyrrhenian Sea. Bound.-Layer Meteorol. 139 (2), 353–366. https://doi.org/10.1007/s10546-010-9577-x.

Pichelli, E., Ferretti, R., Cacciani, M., Siani, A.M., Ciardini, V., Di Iorio, T., 2014. The role of urban boundary layer investigated with high-resolution models and ground-based observations in Rome area: a step towards understanding parameterization potentialities. Atmos. Measure. Techniques 7 (1), 315. https://doi.org/10.5194/amt-7-315-2014.

Rimetz-Planchon, J., Perdrix, E., Sobanska, S., Brémard, C., 2008. PM10 air quality variations in an urbanized and industrialized harbor. Atmos. Environ. 42 (31), 7274–7283. https://doi.org/10.1016/j.atmosenv.2008.07.005.

Schreier, S.F., Richter, A., Peters, E., Ostendorf, M., Schmalwieser, A.W., Weihs, P., Burrows, J.P., 2020. Dual ground-based MAX-DOAS observations in Vienna, Austria: evaluation of horizontal and temporal NO2, HCHO, and CHOCHO distributions and comparison with independent data sets. Atmos. Environ. 5, 100059. https://doi.org/10.1016/j.aeaoa.2019.100059.

Senghor, H., Machu, É., Durán, L., Jenkins, G.S., Gaye, A.T., 2020. Seasonal behavior of aerosol vertical concentration in Dakar and role played by the sea-breeze. Open J. Air Pollut. 9 (1), 11–26. https://doi.org/10.4236/ojap.2020.91002.

Simpson John, E., 1994. Sea Breeze and Local Winds. Cambridge University Press.

Spinei, E., Tiefengraber, M., Müller, M., Cede, A., Berkhout, S., Dong, Y., Nowak, N., 2021. Simple retrieval of atmospheric trace gas vertical concentration profiles from multi-axis DOAS observations (in preparation).

Srinivas, C.V., Venkatesan, R., Somayaji, K.M., Singh, A.B., 2006. A numerical study of sea breeze circulation observed at a tropical site Kalpakkam on the east coast of India, under different synoptic flow situations. J. Earth Syst. Sci. 115 (5), 557–574. https://doi.org/10.1007/BF02702909.

Talbot, C., Augustin, P., Leroy, C., Willart, V., Delbarre, H., Khomenko, G., 2007. Impact of a sea breeze on the boundary-layer dynamics and the atmospheric stratification in a coastal area of the North Sea. Bound.-Layer Meteorol. 125 (1), 133–154. https://doi.org/10.1007/s10546-007-9185-6.

Thompson, W.T., Holt, T., Pullen, J., 2007. Investigation of a sea breeze front in an urban environment. Q. J. R. Meteorol. Soc. 133 (624), 579–594. https://doi.org/10.1002/qj.52.

Wallace, J.M., Hobbs, P.V., 2006. Atmospheric Science: An Introductory Survey, vol. 92. Elsevier.

Yamamoto, Y., Ishikawa, H., 2020. Influence of urban spatial configuration and sea breeze on land surface temperature on summer clear-sky days. Urban Clim. 31, 100578. https://doi.org/10.1016/j.uclim.2019.100578.

Yoshikado, H., 1994. Interaction of the sea breeze with urban heat islands of different sizes and locations. J. Meteor. Soc. Jpn Ser. II 72 (1), 139–143. https://doi.org/10.2151/jmsj1965.72.1_139.